Friedrich-Schiller-University of Jena
Faculty of Physics and Astronomy

FREE-SPACE QUANTUM TELEPORTATION OVER 143-KILOMETERS

Master's thesis

In partial fulfillment of the requirements for the degree of
Master of Photonics

This work was conducted in
the Institute for Quantum Optics and Quantum Information
of the Austrian Academy of Sciences

submitted by

Daqing Wang

Jena, September 2012

I hereby certify that this master thesis has been composed by myself. It describes my own work, or the team work where I worked as a part, unless otherwise acknowledged in the text. The work described in this thesis has not been submitted to meet the requirements of a degree at this or any other institution.

__________, ____________________

Place, Date

____

Signature

Reviewer:

Prof. Dr. Holger Gies

Institute of Theoretical Physics
Friedrich-Schiller-University of Jena
& Helmholtz Institute Jena
Max-Wien Platz 1
D-07743 Jena
Germany

Dr. Rupert Ursin

Institut for Quantum Optics and Quantum Information
Austrian Academy of Sciences
Boltzmanngasse 3
A-1090 Vienna
Austria

Abstract

Quantum teleportation allows the transfer of unknown quantum states over arbitrary distances. Since its first experimental demonstration with photons, quantum teleportation has been realized using varies quantum systems, and with extending distances. In this work, we present the implementing and post-processing of a quantum teleportation experiment with photons, over a 143 km free-space link, between the two Canary Islands of La Palma and Tenerife. As a result, we achieved an average teleportation process fidelity of 0.710(42). Compared with previous experiments on the Canary Islands with one or two photons, the four-photon teleportation experiment is of more technical difficulties due to the reduction of coincidence count rates, which results in a dramatically reduced signal-to-noise ratio. For tackling these problems, we developed a bright frequency-uncorrelated entangled-photon source, a pair of ultra-low-noise large-sensitive-area single photon detectors, and a closed-loop-tracking system to stabilize the free-space link. On the other hand, we paid more attention on the signal analysis, which helped us synchronize the two sites and identify successful teleportation events. A set of studies on the signal analysis were done after the experiment, aiming at optimizing the data processing methods, studying the properties of the free-space channel and providing guidelines for our future experiments.

In this work, we will first give an introduction to the theoretical proposal and previous experimental realizations of quantum teleportation. Then we will talk about the design, setting-up and operating of our teleportation experiment. Later, special attention will be paid on the signal analysis techniques.

Contents

List of figures **5**

List of tables **9**

1 Quantum entanglement and teleportation **11**

1.1 Quantum entanglement . . . 11
1.2 The idea of quantum teleportation . . . 12
1.3 Experimental explorations . . . 14
1.3.1 First teleportation experiment . . . 14
1.3.2 Steps toward long distance teleportation . . . 15
1.3.3 Experiment in present . . . 16

2 Experimental setup **19**

2.1 Spontaneous parametric down conversion (SPDC) . . . 19
2.2 Frequency-uncorrelated SPDC source . . . 21
2.3 Bell-state analyzer . . . 23
2.4 Single photon detectors . . . 24
2.5 Feed-forward channel . . . 26
2.6 Electro-optic modulator (EOM) switching . . . 28
2.7 Complete optical setup . . . 28
2.7.1 Alice at La Palma . . . 28
2.7.2 Bob at Tenerife . . . 30

3 Key techniques **33**

3.1 Tracking . . . 33
3.2 Implementation of feed-forward . . . 34
3.2.1 Coding methods . . . 34
3.2.2 Proof tests in Vienna . . . 36
3.2.3 Delay finding . . . 37
3.3 Detector alignment . . . 38
3.4 Electronics . . . 40

4 Measurement results **41**
4.1 Local performance of the teleportation setup . . . 41
4.2 Measurement results of the inter-island experiment . . . 41

5 Signal analysis **45**
5.1 Data recording . . . 45
5.2 Data flow . . . 46
5.3 Coincidence searching . . . 47
5.4 Clock synchronization . . . 48
5.4.1 Limitations on timing accuracy . . . 49
5.4.2 GPS clock . . . 49
5.4.3 Synchronization based on two-fold coincidences . . . 49
5.5 SNR and coincidence window size . . . 50
5.6 Scintillation . . . 52
5.7 Sunrise . . . 53
5.8 Channel statistics at long time scale . . . 54

6 Conclusion and outlook **57**

Acknowledgements **58**

Appendix **61**

A C++ codes **61**
A.1 source code: readoutChannels.cpp . . . 61
A.2 source code: eraseTaggerBlocks.cpp . . . 65
A.3 source code: processingCSVFiles.cpp . . . 70

B Steps on building up a receiver's module in the OGS **75**

C Steps on operating the OGS tracking system **77**

Bibliography **79**

List of Figures

1.1 Schematic description of the teleportation protocol. 13

1.2 Setup of the Innsbruck97 teleportation experiment. Picture taken from [9]. . 14

1.3 Experiment teleporting polarization state of photons over a 143 km free-space channel, between two islands, La Palma and Tenerife on the Atlantic Ocean. Picture taken from [28]. 16

1.4 Satellite picture of the NOT and JKT at Observatorio del Roque de los Muchachos in La Palma. The two telescopes are separated with approximately 800 meters from each other. Picture taken from http://maps.google.com. 17

2.1 SPDC emission cones in type II phase-matching condition. Picture on the left shows the non-collinear emission. Picture on the right refers to collinear emission. 20

2.2 Setup to prepare arbitrary one of the four Bell-state with non-collinear type II SPDC inside a β-barium borate (BBO) crystal. 20

2.3 Heralded single photon source with type I phase-matching. Detection of the o photon heralds the presence of the e photon. The e photon was used as the teleportation input. 21

2.4 A setup to spatially separate the o and e photons generated via type II SPDC. By using a HWP on one arm of the SPDC source, and recombining both arms with a polarization-beam-splitter (PBS), one can deterministically separate the o and e photons, which have different bandwidths and spatial mode shapes. 22

2.5 Bell-state analyzer with passive linear optical elements. By applying slight modifications, this setup can be changed to differentiate any two of the four Bell-states. Note that, in our real setup, all the photons were coupled into single-mode fibers and interfered inside a fiber beam splitter. 24

2.6 A picture of a decapsulated Perkin Elmer avalanche photodiode, taken from http://www.vad1.com. 25

2.7 Spatial quantum efficiency distribution of the Perkin Elmer C30902SH APD. The spatial profile has a FWHM diameter of 510 μm. 25

2.8 The peaks around 1 μs show the after-pulsing of the two receiver's detectors. 26

2.9 A set of three sending telescopes for feed-forward. 27

2.10 A schematic description of the geometry of the transversal Pockels cells. The two RTP crystals are biased with voltages of opposite sign, and orientated in a way that their z-axes are in 90° to each other. 28
2.11 An overview of complete optical setup on the two islands. Picture taken from [28]. 29
2.12 A picture of the teleportation sources built up in the Jacobus Kapteyn Telescope at La Palma. Picture taken by the co-authors of [28]. 30
2.13 Schematic description of the receiver's setup in Tenerife. 31
2.14 A picture of the actual receiver setup deployed out of the Coude path of the OGS telescope. Picture taken by the co-authors of [28]. 31

3.1 A picture of the tracking laser sent out from the laboratory in Jacobus Kapteyn Telescope at La Palma, taken by the co-authors of [28]. 33
3.2 Trace of the tracking point on the OGS tracking camera at Tenerife over 100 minutes. We can find the long-term drifts in one direction can be successfully avoided with the tracking. The pixel size of the CCD camera is 4.5 μm. . . . 34
3.3 Coding schemes. 35
3.4 Oscilloscope screenshot of the detected signal of logic "1" by a photodiode in single-double-pulse coding. A description of the double-threshold discrimination is sketched. 35
3.5 A 10 km (round-trip) free-space link in Vienna. 36
3.6 Coincidences between the feed-forward pulses and the single photons. The graph on top is from the measurement without the 50 m fiber. The graph downside is from the measurement after the 50 m fiber was plugged in. 37
3.7 Two-fold coincidences between single-photon detection events in La Palma and Tenerife. The reduction of peak value from the upper graph (without the 50 m fiber) and the lower graph (with 50 m fiber) reveals the induced attenuation. 38
3.8 Fluctuation of the counts rates of the H- and the V-detector in Tenerife over 40 seconds, when the position of both detectors are fixed. The count rates of each detector are fluctuating but their ratio (green line) remains stable. . . . 39
3.9 Interconnections of the electronics. 40

4.1 State tomography results (without feed-forward operations) of the four quantum states over the 143 km free-space channel. The bar graphs show the reconstructed density matrices ρ for the four states teleported from Alice (La Palma) to Bob (Tenerife). The wire grids indicate the expected values for the ideal cases. The data shown comprise a total of 605 four-fold coincidence counts in about 6.5 hours. The uncertainties in state fidelities extracted from these density matrices are calculated using a Monte-Carlo routine assuming Poissonian error. Picture taken from [28]. 42

4.2 State fidelity results for the four unbiased-basis states teleported from La Palma to Tenerife. Error bars are given by Poissonian statistics. Picture taken from [28]. 43

4.3 The real-part and the imaginary-part **a** and **b** of the reconstructed quantum process matrix. As expected, the dominant component of σ_0 is the contribution of the identity operation, yielding an overall process fidelity $f_{process}$ = 0.710(42). Picture taken from [28]. 43

5.1 Format of the time-taggers. Each time-tagger is consisting of 16 bytes. 45

5.2 Flow of data processing. 47

5.3 Coincidence peaks generated with the coincidence searching program. The central peaks refers to the “signal” coincidence peak, i.e., generated by the photons in the same down-convertion pair. The side peaks were generated by photons coming from different UV pulses, we refer them to “noise” peaks. . . 48

5.4 Thunderbolt® E GPS Disciplined Clock. The disciplined 1PPS pulses can provide synchronization between separated sites, with accuracy between 10 to 15 ns. Picture taken from http://www.trimble.com. 50

5.5 The upper graph shows the two-fold coincidence peak, which indicates the precise shift between the individual time bases at La Palma and Tenerife. The lower graph shows the corresponding four-fold peak at the very same time position. 50

5.6 SNR with respect to the size of coincidence window. Here the red line “coincidences” stands for the value of central coincidence peak (signal), and the green line “Bkg coincidences” represents the background coincidences (noise). The blue line “SNR” means the ratio of signal to noise. 51

5.7 Count rates of the two Tenerife detectors over 6 s time interval. Sampled every 50 ms. Here, we can clearly see the fast fluctuations introduced by the scintillation. 52

5.8 Histogram of the probability of occurrences of the two detectors’ count rates. 53

5.9 With the increase of the threshold count rate up to 120 counts per 50 ms (2400 Hz), the four-fold teleportation visibility increased from 75% to 92%. The loss of counts due to the distillation is expressed in terms of attenuation (dB). Due to the induced attenuation, the total number of effective counts is decreasing with the threshold, results in an growing error bar of the four-fold visibility. . 54

5.10 Single count rates, coincidences and SNR at sunrise time in the ninth measurement night. 55

5.11 The local two-fold coincidence rates in Tenerife, and the seeing data collected by the OGS tracking system at the same measurement time. Sampled with running average of 4 minutes. 56

B.1 Optical design of the Optical Ground Station (OGS) and the receiver's module in Tenerife. Taken from [40]. 76

C.1 Screenshot of the control software of the OGS tracking system. 78

List of Tables

3.1 Testing results of the four coding methods. Here "Dbl. Pl. 1 (2)" stands for single-double-pulse coding with single (double) discrimination threshold(s). "Commu. Eff." represents the communication efficiency of the coding schemes. "Pl. Length" means the length of the electronic triggering signal. "El. Delay" stands for the total delay for encoding, detection, and decoding. 36

4.1 Local performance of the teleportation setup. 41

5.1 Data recording in La Palma and Tenerife. Here GPS 1PPS pulses refers to the one-pulse per second (1PPS) signal from the Global Positioning System (GPS) clock module, which were used in the coarse synchronization of the clock. 46

5.2 Variables in the coincidence searching program. 47

Chapter 1

Quantum entanglement and teleportation

1.1 Quantum entanglement

Entanglement lies on the heart of quantum sciences. It forms the basis of many most remarkable quantum phenomenons and enables the application of quantum science in communication, computation, etc. Entanglement describes the non-classical correlation between dual or multi particles, in such a state that they cannot be interpreted independently from each other. As introduced by Einstein, Podolsky and Rosen [1], it was initially used to prove that quantum mechanics cannot completely describe the physical world. In their original paper, the authors based their arguments on the "element of reality", which indicates that the measurement result of a physical system is determined in prior and independent from the measurement itself. Such that entanglement was shown as an example which conflicts with the "local realism" interpretation. This opened the physical and philosophical debate on whether quantum mechanics is complete, and for nearly 30 years no definite answer was reached. In 1964, a mathematical formulation of this debate, an inequality was proposed by Bell [2]. This provides a criterion for the experimental verification of this debate. However, due to limited experimental resources, the first "Bell" experiment was performed 20 year later by Freedman and Clauser [3]. Followed by several remarkable "Bell" experiments by Aspect *et al.* [4, 5, 6], the bound of classical description was clearly suppressed. However, a definitive "loophole-free" Bell experiment would still be on demanding to faithfully prove the completeness of quantum mechanics. Since the arguments about the "loopholes" are not closely related with the work presented here, we will not put too many details here.

In the description of quantum mechanics, entanglement can be defined with a composite system, whose state cannot be described by a tensor product of each individual state. Consider the case of a two-particle system, we denote the state of each particle as $|\psi\rangle_A$, $|\psi\rangle_B$. If

$$|\psi\rangle_{AB} \neq |\psi\rangle_A \otimes |\psi\rangle_B, \tag{1.1}$$

we say particle A and B are entangled. This means each particle in this composite system cannot be interpreted independently from the other. They have strong correlations with each other which can be independent from their separations in physical space. For two-particle entanglement, the four maximally-entangled states are:

$$|\psi^{\pm}\rangle_{AB} = \frac{1}{\sqrt{2}}(|0\rangle_A|1\rangle_B \pm |1\rangle_A|0\rangle_B), \tag{1.2}$$

$$|\varphi^{\pm}\rangle_{AB} = \frac{1}{\sqrt{2}}(|0\rangle_A|0\rangle_B \pm |1\rangle_A|1\rangle_B), \tag{1.3}$$

which are called "Bell-states". Here $|0\rangle_A$ ($|0\rangle_B$) and $|1\rangle_A$ ($|1\rangle_B$) describes the eigen-states of particle A (B), and are mutually orthogonal to each other. Bell-states are the basis of many purely-quantum phenomenons, among which, "quantum teleportation" is the most striking one for a "classical" mind.

1.2 The idea of quantum teleportation

The word "teleportation" is normally found out in science fictions and fairy tales, which means "to make a person or object disappear while an exact replica appears somewhere else" [7]. In 1993, Bennet *et al.* proposed a scheme which can "teleport" the quantum state of a particle. With the assistance of a Bell-state and a classical channel, one can teleport the state of a quantum system to a partner who can be arbitrarily far away or even at an unknown place, namely "quantum teleportation" [7].

In their proposal, the authors considered two parties, Alice and Bob, who can essentially be separated by an arbitrary distance, share a pair of entangled spin-1/2 particles, particle 2 and 3, in a Bell-singlet state

$$|\psi^-\rangle_{23} = \frac{1}{\sqrt{2}}(|\uparrow\rangle_2|\downarrow\rangle_3 - |\downarrow\rangle_2|\uparrow\rangle_3), \tag{1.4}$$

where $|\uparrow\rangle$ ($|\downarrow\rangle$) denotes the spin-up (spin-down) state of the particle. The sender, Alice, wants to teleport the quantum state of a particle (particle 1) to the receiver, Bob. The state of particle 1 can be written as

$$|\Phi\rangle_1 = \alpha|\uparrow\rangle_1 + \beta|\downarrow\rangle_1. \tag{1.5}$$

Here α and β satisfy $|\alpha|^2 + |\beta|^2 = 1$. Note that the state $|\Phi\rangle_1$ can be arbitrary and unknown to neither Alice nor Bob.

To realize the teleportation, Alice needs to perform a joint Bell-state measurement (BSM) on the input particle 1, and her part of the shared entangled pair, particle 2. The state of the three-particle system can be written as

$$\begin{aligned}
|\Psi\rangle_{123} &= (\alpha|\uparrow\rangle_1 + \beta|\downarrow\rangle_1) \otimes \frac{1}{\sqrt{2}}(|\uparrow\rangle_2|\downarrow\rangle_3 - |\downarrow\rangle_2|\uparrow\rangle_3) \\
&= \frac{1}{2}[|\psi^-\rangle_{12} \otimes (-\alpha|\uparrow\rangle_3 - \beta|\downarrow\rangle_3) \\
&\quad +|\psi^+\rangle_{12} \otimes (-\alpha|\uparrow\rangle_3 + \beta|\downarrow\rangle_3) \\
&\quad +|\phi^-\rangle_{12} \otimes (\beta|\uparrow\rangle_3 + \alpha|\downarrow\rangle_3) \\
&\quad +|\phi^+\rangle_{12} \otimes (\beta|\uparrow\rangle_3 - \alpha|\downarrow\rangle_3)]. \qquad (1.6)
\end{aligned}$$

As seen in Eq.[1.6], Alice will randomly observe one out of the four Bell-states, $|\psi^\pm\rangle_{12}$ or $|\phi^\pm\rangle_{12}$, each with equal probability of 25%. The BSM will project particle 3 onto a state which already contains all the information of particle 1, except for a flip of the basis state depending on which Bell-state was observed. Therefore, Alice must communicate via classical means to Bob which state she observed in her BSM and Bob has to perform a corresponding unitary transformation on particle 3 to obtain an exact replica of Alice's input particle 1. This step is called feed-forward.

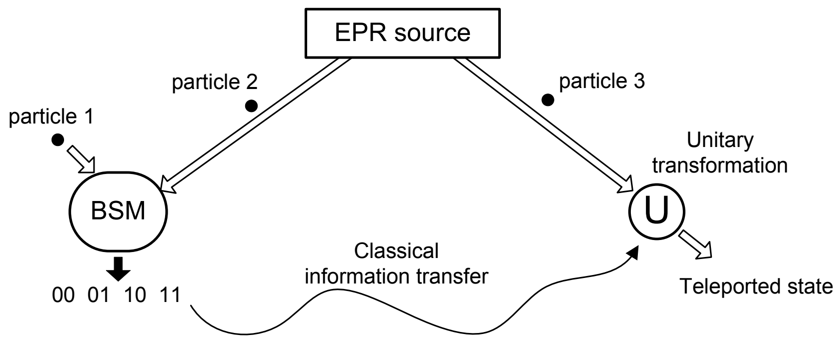

Figure 1.1: Schematic description of the teleportation protocol.

If Alice detects a $|\psi^-\rangle_{12}$ in the BSM, the state of particle 3 will be the same as the initial state $\alpha|\uparrow\rangle_1 + \beta|\downarrow\rangle_1$ of particle 1 except for an irrelevant global phase factor. Therefore Bob does not need to do anything to complete the teleportation. Otherwise, if Alice detects $|\psi^+\rangle_{12}$, Bob will get the state $-\alpha|\uparrow\rangle_3 + \beta|\downarrow\rangle_3$ and thus he has to apply a relative π phase shift between the spin components $|\uparrow\rangle$ and $|\downarrow\rangle$ to convert the state of particle 3 into the original state of particle 1. Otherwise, if Alice obtains the results $|\phi^-\rangle_{12}$ or $|\phi^+\rangle_{12}$, Bob needs to apply both a bit-flip operation (i.e. flip up to down spin and vice versa) and a 0 or π phase shift. The flow of quantum teleportation protocol is shown in Fig.1.1.

So, by utilizing an entangled pair and sending two bits of information over a classical channel, Alice can teleport an unknown quantum state to another party, Bob, who can be arbitrarily far away or even at a place unknown to Alice.

1.3 Experimental explorations

1.3.1 First teleportation experiment

After the theoretical proposal, intensive interests were raised on the experimental verification and realization of quantum teleportation. The first experimental demonstration of quantum teleportation was done in 1997 by Bouwmeester *et al.* in Innsbruck [8]. The experiment utilized four photons generated via spontaneous parametric down conversion (SPDC), and teleported the polarization state of the photons.

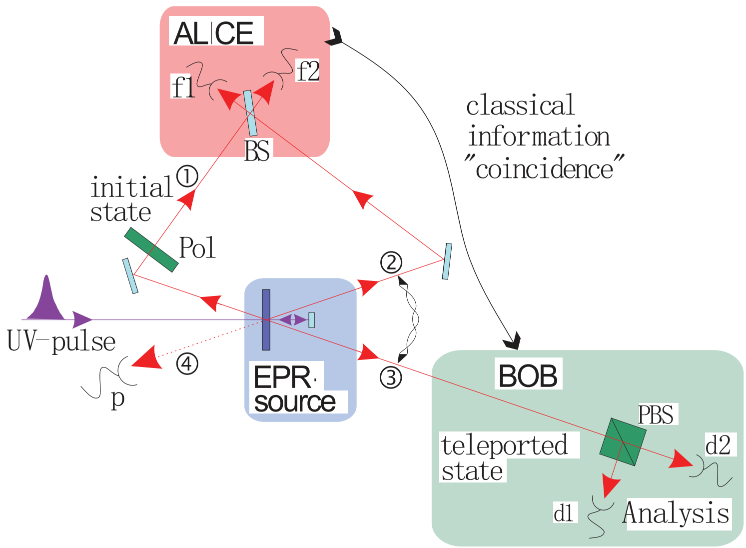

Figure 1.2: Setup of the Innsbruck97 teleportation experiment. Picture taken from [9].

The original setup of the Innsbruck experiment is shown in Fig.1.2. Ultrafast ultraviolet (UV) pulses at 394 nm were first directed through a β-barium borate (BBO) crystal. On passing through the crystal, with a certain probability one UV photon will be down-converted into a pair of photons at 788 nm, which were entangled in their polarization freedom. The pair, here we call photon 2 and photon 3, was used as shared entanglement between Alice and Bob. After passing through the nonlinear crystal, the UV pulses hit a retro-reflector, propagated backward and went through the BBO crystal again following the incoming path. The same as before, with a certain probability, one UV photon will generate another pair of photons, photon 1 and photon 4. In this experiment, photon 4 was used as a trigger to herald the presence of photon 1, and photon 1 was used to prepare the teleportation input.

To make a combined Bell-state measurement, photon 1 and photon 2 were superposed on a 50:50 beam splitter (BS). A single-photon detector was placed at each output port of the BS. To get a longer coherence time of the two photons, narrow-band interference filters ($\Delta\lambda = 4.6$ nm) were placed in front of the detectors. Note that this BSM setup is only capable to differentiate $|\psi^-\rangle$ out of the other three Bell-states. A $|\psi^-\rangle$ detection corresponds to a two-fold coincidence detection between the two detectors $f1$ and $f2$. A successful teleportation event is confirmed with a three-fold coincidence between the two BSM detectors, and one detector ($d1$ or $d2$) in the polarization analysis setup of photon 3. For example, when the $+45°$ polarized photons are teleported, within the teleportation region there shall only be three-fold coincidences between detectors $d2f1f2$, and no coincidences between detectors $d1f1f2$. By scanning the traveling path length of photon 2, one can find a dip of three-fold coincidences $d1f1f2$. This verifies the teleportation process. As a result, the experiment teleported five states with an average three-fold coincidence visibility of $68\% \pm 1\%$. When consider the four-fold coincidence visibility by including the detection events of photon 4 (excluding the spurious three-fold coincidences), the experiment gave an overall four-fold coincidence visibility of $70\% \pm 3\%$, which clearly surpassed the classical limit of 2/3 [10] and proved the teleportation of single-photon quantum states.

1.3.2 Steps toward long distance teleportation

Shortly after the Innsbruck experiment, another teleportation experiment was reported by Boschi *et al.* in Roma [11]. In their experiment, the teleportation was realized with two photons, using path-polarization entanglement and a BSM scheme to distinguish all the four Bell-states. However, this scheme does not allow a teleportation input photon to come from externally, and the state of the input must be known by someone who runs the setup. This means the "input source" must be known and prepared manually.

Later wards, teleportation was further demonstrated with coherent light [12], with atoms in a trichloroethylene molecule [13], with trapped ions [14], and between a coherent state light and an atomic ensemble [15]. The first experimental trial to perform teleportation at long distance was done by the Geneva group in 2003 [16], with 2 km optical fibers as a quantum channel between two laboratories separated by 55 meters. In 2004, Ursin *et al.* carried quantum teleportation out of the laboratories into "real-world" [17]. The experiment was done with optical fibers across the Danube in Vienna, with a distance of around 600 meters. Since the optical fibers exhibit intrinsic transmission losses per kilometer, as another option, free-space optical channel attracted intensive attention for truly long-distance quantum optical applications [18, 19, 20, 21, 22, 23]. A free-space teleportation experiment over 16 km was reported by a Chinese group [24] in 2008, using a similar scheme with [11]. However, it also has the problem of on externally teleportation input. Since 2007, varies experiments utilizing one or two photons have been done by our group on a 144 km free-space quantum channel between two Canary Islands, La Palma and Tenerife [25, 26, 27]. As a four-photon experiment, quantum teleportation over long-distance free-space channel remained an experimental challenge due to the notably lower coincidence rates compared to two-photon experiments.

1.3.3 Experiment in present

In the following part of this thesis we will talk about an experiment teleporting photonic qubits between two laboratories located on two Canary Islands in the Atlantic Ocean, La Palma and Tenerife, separated by 143 km [28].

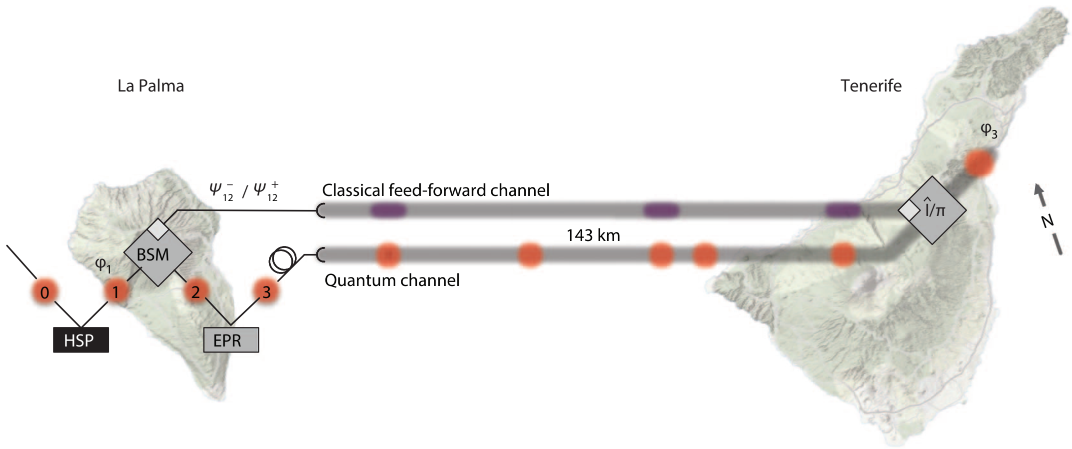

Figure 1.3: Experiment teleporting polarization state of photons over a 143 km free-space channel, between two islands, La Palma and Tenerife on the Atlantic Ocean. Picture taken from [28].

A bright frequency-uncorrelated entangled photon source (EPR) and source for input photons (HSP) were setup in Jacobus Kapteyn Telescope at La Palma, with a BSM setup capable to detect two out of the four Bell-states. The 143 km long free-space channel consisted of a small home-made transmitting telescope in La Palma and a 1 m receiver telescope in Tenerife operated by the European Space Agency (ESA). A classical optical communication channel was also setup to realize real-time feed-forward. After synchronization of the two laboratories using the Global Positioning System (GPS), we were able to identify the four-fold coincidences, which confirm successful teleportation events.

Note that in this experiment we moved to the new sender's laboratory in the Jacobus Kapteyn Telescope (JKT) at La Palma. While our previous inter-island experiment [25, 26, 27] were conducted with the infrastructure affiliated to the Nordic Optical Telescope (NOT), which are approximately 800 meters far away. That's the reason why the link length has a 1 km reduction compared to the previous experiments. A satellite picture of the NOT and JKT is shown in Fig.1.4, and a picture of the new laboratory inside JKT can be found in Fig.2.12.

This thesis is organized as follows. In Chapter 2 we will talk about the experimental setup, first based on each individual functional modules, and then with an overview of the whole optical setup. In Chapter 3 we explain the key techniques employed in the experiment, including tracking, feed-forward, detector alignment, etc. The results of this experiment will be presented in Chapter 4. In Chapter 5 we talk about the signal analysis, the methods for

Figure 1.4: Satellite picture of the NOT and JKT at Observatorio del Roque de los Muchachos in La Palma. The two telescopes are separated with approximately 800 meters from each other. Picture taken from http://maps.google.com.

data recording and processing, the synchronization and the study on the channel properties. Finally we come to a conclusion in Chapter 6.

Chapter 2

Experimental setup

2.1 Spontaneous parametric down conversion (SPDC)

Photons can be entangled in varies degrees of freedom. Since the polarization of a photon can easily be controlled and manipulated with high accuracy, it's now widely used as the degree of freedom for entanglement in quantum optical experiments.

Generation of entangled photons is a core part of photonics quantum information processing. In early experiments, cascaded atoms were used as entanglement photon sources [4, 5, 6, 29]. However, such sources are difficult to handle and prohibit drawbacks like poor emission directionality, low brightness, etc. Later explorations found out that one of the second order nonlinear effects, the spontaneous parametric down conversion (SPDC), can be employed to generate polarization-entangled photons with excellent directionality, high purity and brightness. It has been well studied and becomes a widely used entangled-photon generator [30, 31].

SPDC is stimulated by the interaction of incoming pump light and the vacuum fluctuations inside the medium (normally a nonlinear crystal). As a result, the pump photon will have a probability to split into a pair of “signal” and “idler” photons, following the law of energy conservation and momentum conservation. Refer to different phase-matching conditions, SPDC can be classified to type I and type II. In type I condition, the signal and idler photons have the same polarization. While in type II condition, the polarization of the two photons are orthogonal to each other.

Currently, the common source for polarization entanglement is based on type II SPDC. In case that the nonlinear crystal is cut in a suitable way, the type II down-converted photons are emitted along two cones, which are in centrosymmetry with respect to the direction of the pump beam, As shown in Fig.2.1. Photons emitted in one of the cones are ordinarily (horizontally) polarized, photons in the other cone are extraordinarily (vertically) polarized.

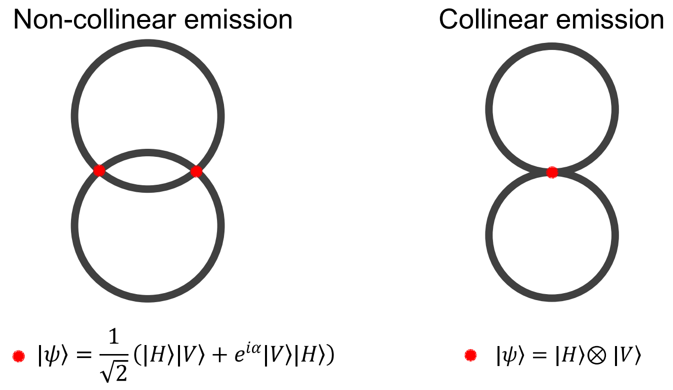

Figure 2.1: SPDC emission cones in type II phase-matching condition. Picture on the left shows the non-collinear emission. Picture on the right refers to collinear emission.

Type II SPDC can be further classified into collinear and non-collinear emission cases, with respect to different ways of crystal cutting. In non-collinear situation, as shown on the left side of Fig.2.1, photons emitted at the two intersection areas of the two cones can be described by an entangled state:

$$|\psi\rangle = \frac{1}{\sqrt{2}}(|H\rangle|V\rangle - e^{i\alpha}|V\rangle|H\rangle). \tag{2.1}$$

Here $|H\rangle$ and $|V\rangle$ denote the horizontal and vertical polarization state of the photon, respectively. The relative phase shift α is induced by the birefringence of the crystal. It can be compensated with a half wave-plate (HWP) and a compensation crystal (which is the same with the down-conversion crystal but with half of the thickness) on each down-conversion arm. The HWP rotates the polarizations by 90°, which exchanges the polarization of the two photons. The compensation crystal will then let one photon experience the same phase shift which the other photon experienced in the first crystal, thus compensate the relative phase shift. Note that, the down conversion process can happen at all penetration depthes inside the first crystal, which is called the longitudinal walk-off effect. The usage of a half-thick crystal is to compensate the average phase shift within all the photon pairs.

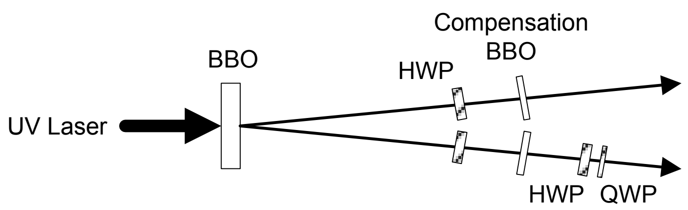

Figure 2.2: Setup to prepare arbitrary one of the four Bell-state with non-collinear type II SPDC inside a β-barium borate (BBO) crystal.

If one further place another set of HWP and quarter-waveplate (QWP) on one of the down-conversion path, all the four maximally-entangled Bell states can be prepared [30]. See

Fig.2.2.

In the case of collinear emission, the photon pairs collected from the intersection point are in a product state of orthogonal polarizations. Despite the absence of entanglement properties, the strong temporal correlation of the two photons still offers a possibility for it to be used as a heralded single photon (HSP) source. That means, the detection of one photon in the pair indicates the presence of the other photon.

Both the non-collinear and the collinear SPDC sources were used in our experiment. The non-collinear SPDC source was used as Bell-state source, to generate photon pairs in state $|\psi^{-}\rangle$ as shared entanglement between Alice and Bob. The collinear SPDC source was used as a HSP source to generate single photons as inputs for the teleportation.

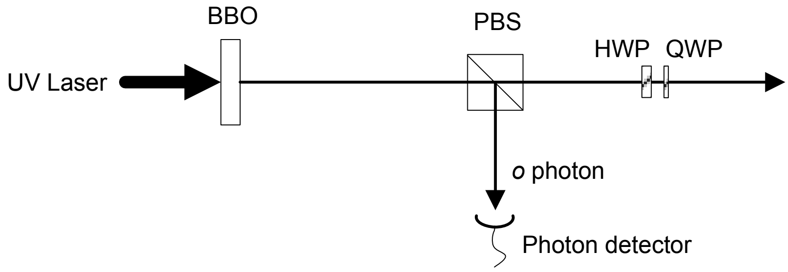

Figure 2.3: Heralded single photon source with type I phase-matching. Detection of the o photon heralds the presence of the e photon. The e photon was used as the teleportation input.

As shown in Fig.2.3, in our HSP source, the two collinearly emitted photons were first separated with a polarization-beam-splitter (PBS). The V-polarized (vertically polarized) ordinary photon (o photon) was reflected and detected with a single photon detector. Detection of the o photon heralds the presence of the H-polarized (horizontally polarized) extraordinary photon (e photon). The e photon was transmitted through the PBS, passed a set of HWP and QWP, through which an arbitrary polarization can be prepared. The e photon with manually prepared polarization was then sent into a Bell-state measurement setup as an externally teleportation input photon. The reason for using an e photon for interference is due to its narrower spectrum with respect to the o photon under pulsed pumping, which results in a longer coherence time.

2.2 Frequency-uncorrelated SPDC source

Following our discussions in the previous section, a bright polarization-entangled photon source can be built up based on type II SPDC with strong continuous pumping. However, in multi-photon experiments one needs to interfere photons from different sources. This further requires the photons to have good timing properties. A straightforward solution for this is to use an ultrafast pulsed pump laser, which can time the photons within femtosecond scale. However, ultrafast pumping also induces a side effect, namely the spectral distinguishability between o and e photons. This means the o photon and e photon can be spectrally distinguishable to each other because their different bandwidths. This results in a reduction of the entanglement quality [32, 33].

Using narrow-band filters to select only the high-quality entangled photons is a traditional way to erase the spectral distinguishability. However, this leads to a significant reduction of the count rates. In normal cases the down-converted photon have a bandwidth of about 7 nm. Applying 1-2 nm bandwidth filters can cause nearly 50% losses on each of the arm.

Recently, schemes for frequency-uncorrelated entangled photon source (FUEPS) were proposed and applied [34, 35], which allows to increase the entanglement quality while maintaining the count rates. Following the scheme by Poh, *et al.* [34], we built up a FUEPS at La Palma as the entangled photon source. A mode-locked Ti:Sapphire laser was used to generate near-infrared femtosecond laser pulses (central wavelength at 808 nm) with a repetition rate of 80 MHz and pulse duration of 140 fs. The 808 nm pulses were up-converted to blue pulses (central wavelength at 404 nm) via second-harmonic-generation inside a BBO crystal. Then the 404 nm pulses went through a BBO crystal, where one 404 nm photon has a probability to be down-converted to a pair of 808 nm photons. Each 808 nm photon pair consists of an o (ordinary, vertically polarized) photon and an e (extraordinary, horizontally-polarized) photon, in an entangled state

$$|\psi^-\rangle = \frac{1}{\sqrt{2}}(|H_e\rangle|V_o\rangle - e^{i\alpha}|V_o\rangle|H_e\rangle). \tag{2.2}$$

A set of waveplates and compensation BBO crystals were used to compensate the relative phase difference α following the scheme in Fig.2.2.

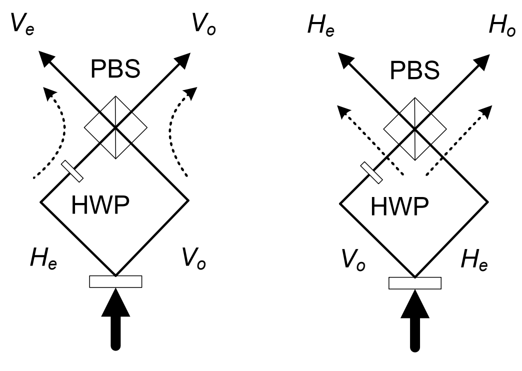

Figure 2.4: A setup to spatially separate the o and e photons generated via type II SPDC. By using a HWP on one arm of the SPDC source, and recombining both arms with a polarization-beam-splitter (PBS), one can deterministically separate the o and e photons, which have different bandwidths and spatial mode shapes.

Afterwards, the two photons went through a setup to spatially separate the o and the e photon (see Fig.2.4). The e photon was then sent to the BSM setup to interfere with the teleportation input photon. The usage of the e photon for the interference is due to its narrower bandwidth, yields a longer coherence time. The spatial separation allows to deterministically interfere the e photon with the teleportation input, thus avoid to use narrow-band filters on both of the arms. The coincidence count rates can also be increased by enhancing the efficiency of the single mode fiber coupling, while maintaining the entanglement quality.

In our experiment, we used an 8 nm interference filter for the o photon, and a 3 nm filter for the e photon. With the 8 nm interference filter, we could increase the 4-fold coincidence rate by approximately 20%.

2.3 Bell-state analyzer

Teleportation requires a combined Bell-state measurement on the input photon and one of the entangled photon. In the experiment we used a passive linear optical Bell-state analyzer. It can differentiate two out of the four Bell-states,

$$|\psi^{\pm}\rangle = \frac{1}{\sqrt{2}}(|H\rangle|V\rangle \pm |V\rangle|H\rangle), \tag{2.3}$$

$$|\varphi^{\pm}\rangle = \frac{1}{\sqrt{2}}(|H\rangle|H\rangle \pm |V\rangle|V\rangle). \tag{2.4}$$

This 50% efficiency is the optimum achievable with linear optical elements [36].

In this analyzer, as seen from Fig.2.5, the two incoming photons interfere at the 50:50 beam splitter (BS). If the two photons have symmetric phases ($|\psi^+\rangle, |\phi^{\pm}\rangle$), they will come out at the same output port of the BS. If the photons are anti-symmetrically phased, the will come out at different output ports. Two polarization beam splitter (PBS) and two sets of detectors (D_a and D_b, D_c and D_d) were placed at the outputs of the BS, to analyze the polarization of the photons.

When two photons in state $|\psi^-\rangle$ coming in the setup, they will come out at different ports on the BS since they have anti-symmetric phases. Also, the two photons have orthogonal polarizations, which let them come out at different ports of the PBSs. So, they will generate a coincidence detection event between detectors D_a and D_c, or between detectors D_b and D_d. Similarly, two photons in state $|\psi^+\rangle$ will generate a coincidence detection event between D_a and D_b, or between D_c and D_d. States $|\phi^{\pm}\rangle$ are not distinguishable from each other with this setting, since the photons in these two states will hit the same detector and their relative phase is unknown.

Note that, in our experiment, before the BSM, all photons were spectrally filtered and coupled into single-mode fibers for spatial mode selection. Alice's photon 2 (e photon) was set to

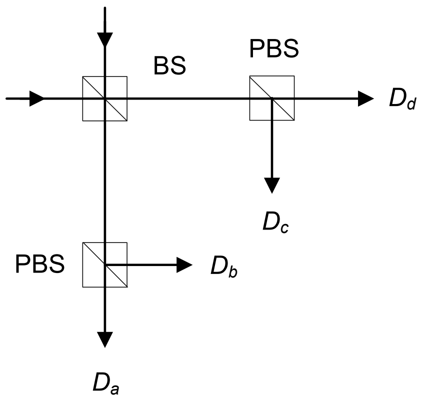

Figure 2.5: Bell-state analyzer with passive linear optical elements. By applying slight modifications, this setup can be changed to differentiate any two of the four Bell-states. Note that, in our real setup, all the photons were coupled into single-mode fibers and interfered inside a fiber beam splitter.

overlap in a fiber beam splitter (FBS) with the teleportation input photon 1 (e photon).

2.4 Single photon detectors

Nowadays, the most widely used single photon detectors are built up from silicon avalanche photodiodes (Si-APDs). In such detectors, there exist a tradeoff between the dark count rate and the size of sensitive area. Commercial low noise detectors (dark count rate<10 Hz) normally have limited detection area (diameter <100 μm). However, in free-space experiments we have demands on optimizing both parameters. As we calculated, the achievable focal spot out of the Coude focus of the OGS telescope is with around 300 μm diameter. This requires the receiver's photon-detector to have a diameter larger than 300 μm. Also, due to the strong link attenuation (28 to 39 dB), the received single photon rates at Tenerife can easily be comparable with the background noise. Thus the detector should also have achievable low dark count rate.

In collaboration with Vadim Markarov from the University of Waterloo, we set up a set of ultra-cold single-photon detectors [37] in our experiment. The detectors were designed based on Perkin Elmer C30902SH APDs, with a 500 μm-diameter sensitive area. See Fig.2.6 and Fig.2.7. Four-stage thermoelectric coolers were used to cool the APDs down to -70 ℃. This reduces the dark count rates down to 10 to 20 Hz.

A drawback for cooling the APDs further down is the increasing after-pulsing effect with the decreasing of temperature. To make clear how strong the after-pulsing of our detectors is, we performed an 8-hour test in darkness, with all possible light sources shielded.

Since the detectors were working in darkness, all the count events were registered by dark

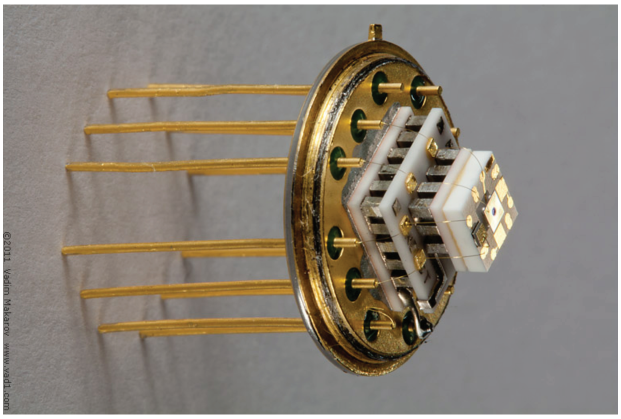

Figure 2.6: A picture of a decapsulated Perkin Elmer avalanche photodiode, taken from http://www.vad1.com.

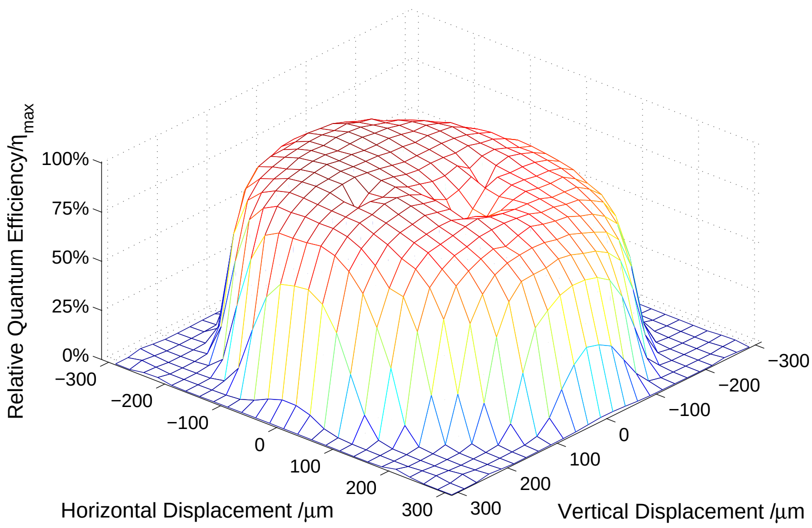

Figure 2.7: Spatial quantum efficiency distribution of the Perkin Elmer C30902SH APD. The spatial profile has a FWHM diameter of 510 μm.

counts and after-pulses. We based our analysis on sampling the occurrence of time separation between two successive counting events. Giving that after-pulse appears shortly after the click of a photon (or dark count) and generate another click, the presence of after-pulsing will be indicated by a dominate occurrence peak, at a time directly after the detector dead-time and much earlier than the average separation between dark counts (1/16Hz≈62.5 ms).

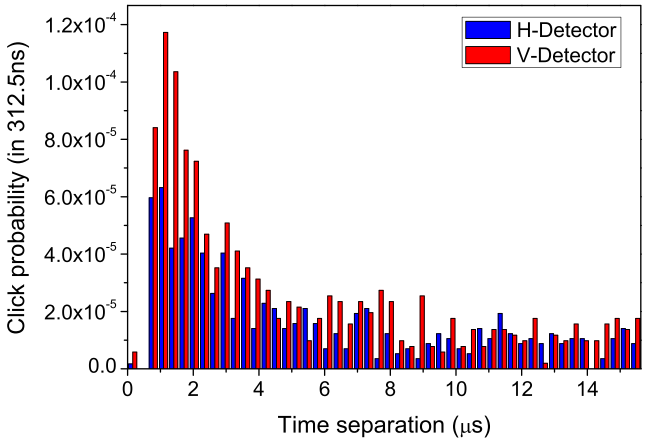

Figure 2.8: The peaks around 1 μs show the after-pulsing of the two receiver's detectors.

Results of the analysis are shown in Fig.2.8. The x-axis is the time separation with respect to the previous detection event. The y-axis is the probability of finding an adjacent detection event within a period of 312.5 ns centered at time x. We can find there is only neglectable probability to find an adjacent detection event within 0.8 μs time separation. This confirms that the detectors have a dead-time of around 0.8 μs. The after-pulsing peak is showing up in between 1 μs and 4 μs. The dark count rates of the two detectors were measured to be 16.0 Hz (V-detector), and 17.8 Hz (H-detector). Given the low click probability, the after-pulsing would not surpass the dark counts in low count rates regime (kilohertz level).

2.5 Feed-forward channel

The finalization of quantum teleportation requires Alice to send her BSM result to Bob via a classical channel. On receiving this information, Bob performs a corresponding unitary transformation on her quantum state, which turns the state to the same state with the teleportation input. This process is called feed-forward.

In our experiment, we employed a classical optical communication channel which encodes the BSM results onto sequences of laser pulses to real-timely feed the BSM results to Bob. At La Palma, three identical 1064 nm lasers were used as the sender. The three lasers were triggered with the same electrical signal. Three 7 cm aperture telescopes were used to sent out the emitted light. The aim of using three sending apparatus is to construct a set of incoherent sending apertures, such that the out-sent signal will be more robust against the turbulence. For the same reason, we tried to mount the telescopes as far away from each other as possible during the Canary experiments. The three telescopes in the lab test in Vienna are shown in Fig.2.9.

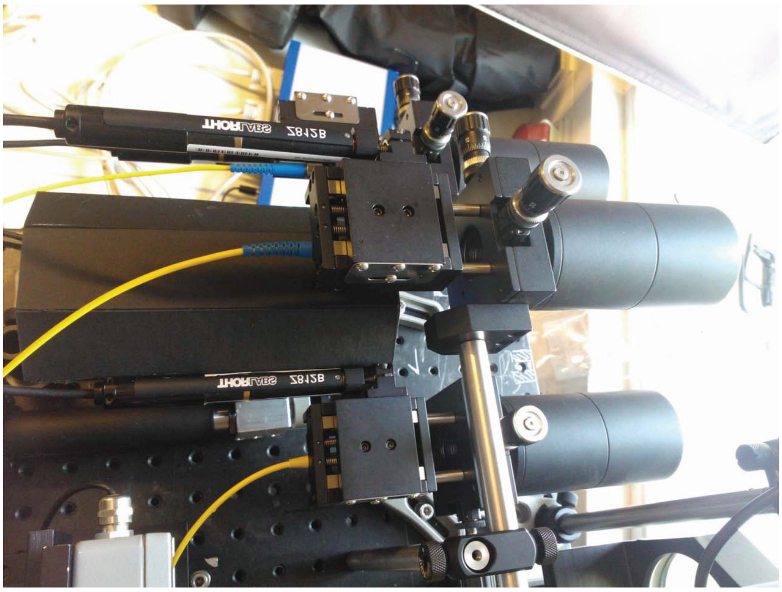

Figure 2.9: A set of three sending telescopes for feed-forward.

At Tenerife, the feed-forward signal was collected together with the quantum signal and the tracking laser. We used two dichroic mirrors to separate the three sets of signals, and a $f = 40$ cm lens to focus the feed-forward signal onto a photodiode. A threshold voltage was set to the output of the photodiode to discriminate the incoming of a pulse. The sequences of discriminated signal were further analyzed by a decoder, to finally identify the information sent by Alice. Once a $|\psi^+\rangle$ is decoded, a triggering signal will be sent to the Pockels cells, to perform an unitary transformation on the incoming quantum signal.

Since the feed-forward signal and the quantum signal travel with nearly the same speed in the atmosphere, to leave sufficient time for Bob to be ready for the unitary transformation, one must apply a delay to the quantum signal. Thus we coupled the quantum signal into a 50 m optical fiber in the La Palma laboratory, which led to a 250 ns delayed coming with respect to the feed-forward signal. This delay is longer enough for Bob to finish the unitary transformation.

2.6 Electro-optic modulator (EOM) switching

The unitary transformation at Bob's side was realized with a set of Pockels cells. A Pockels cell can work as a voltage-controlled waveplate. By applying a variable electric voltage on the Pockels cell, one can modify the refractive index of the crystal along different crystal axes, and thus modulate the polarization of the light propagating through. This process is also called EOM switching.

In our experiment, we used a set of transversal Pockels cells produced by Leysop LTD, consisted of two $4 \times 4 \times 10$ mm Rubidium Titanyl Phosphate (RTP) crystals placed in sequence with respect to the beam path. The Pockels cells are called transversal because the crystals were cut in a way that the beam path is along the crystallographic y-axis, which is perpendicular to the applied voltage along the z-axis. The crystal is exhibiting birefringence to the beam propagating along y-axis even in the absence of an electrical field. The usage of two RTP crystal is to compensate this zero-voltage birefringence by orienting them with their z-axes in 90° to each other. The voltages applied on the two crystals are in opposite sign, such that this compensation will not appear during the switching operations. A schematic description of the geometry of Pockel cells is shown in Fig.2.10. A splitter box is used to generate the triggering signal for the two crystals to perform switching operation.

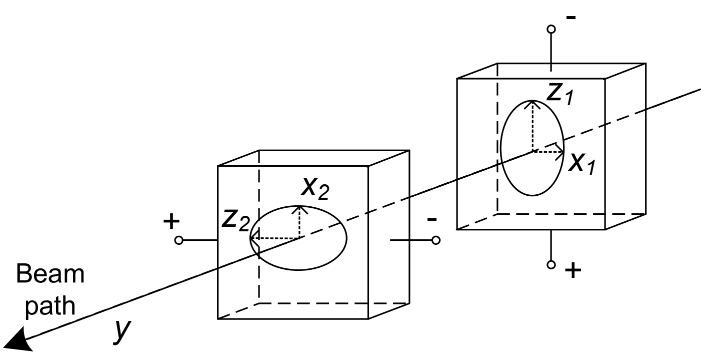

Figure 2.10: A schematic description of the geometry of the transversal Pockels cells. The two RTP crystals are biased with voltages of opposite sign, and orientated in a way that their z-axes are in 90° to each other.

2.7 Complete optical setup

2.7.1 Alice at La Palma

Based on our discussions on individual modules, here we give an overview of the complete optical setup deployed on the two islands.

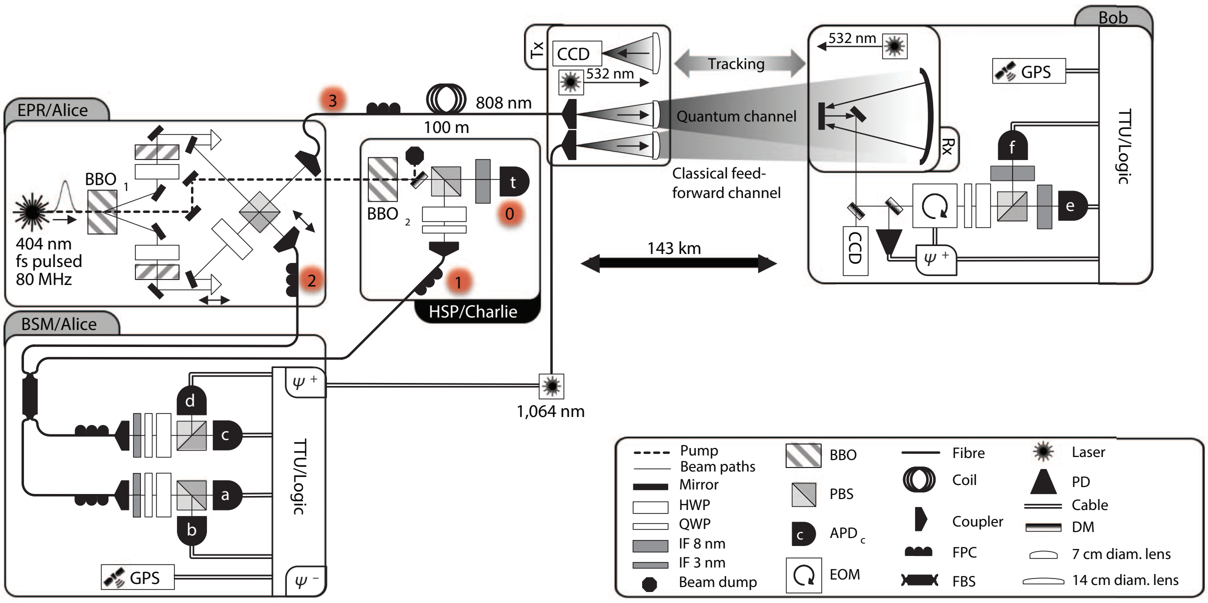

Figure 2.11: An overview of complete optical setup on the two islands. Picture taken from [28].

As seen from Fig.2.11, in La Palma, the ultrafast laser pulses at 808 nm were first up-converted to 404 nm inside a nonlinear crystal. The 404 nm pulses were directed to a BBO crystal (BBO_1) as a pump. In combination with a HWP and a PBS, a FUEPS (EPR/Alice) was constructed with the down-converted photons from BBO_1. We denote the two out coming photons from the FUEPS as photon 2 (e photon) and 3 (o photon).

After passing through BBO_1, the 404 nm pulses went through a second BBO crystal (BBO_2), which worked as a HSP source (HSP/Charlie). The crystal was polished to deliver pairs of horizontally and vertically polarized photons in a product state. Here we note as photons 0 (o photon, V-polarized) and photon 1 (e photon, H-polarized). The two photons were separated by a PBS. A single photon detector t was placed to detect photon 0. The detection served as a trigger to herald the presence of photon 1.

All the four photons were coupled into single-mode fibers. Photons 1 and 2 then interfered in a fiber beam splitter (FBS) followed by two PBSs and four single photon detectors (BSM/Alice). At the same time, photon 3 was guided to the transmitter telescope via a 50 m single-mode fiber and sent to Bob.

Directly after the BSM, the result was encoded in the 1064 nm laser pulses and sent to Bob. The 50 m fiber ensures that there was enough time for Bob to be ready for applying an unitary transformation before the quantum signal arrives. Fig.2.12 is a picture of the sender's laboratory inside the Jacobus Kapteyn Telescope.

Figure 2.12: A picture of the teleportation sources built up in the Jacobus Kapteyn Telescope at La Palma. Picture taken by the co-authors of [28].

2.7.2 Bob at Tenerife

At Tenerife, there were in total three sets of incoming signals: the tracking signal at 532 nm; the quantum signal at 808 nm; and the feed-forward signal at 1064 nm. All three sets of signals were collected by the 1 m aperture OGS telescope, guided through its Coude path to Bob. Two dichroic mirrors (DMs) were used to separate the signals. See Fig.2.13. At the first DM (DM1), the quantum signal was reflected, then collimated by a $f = 40$ cm lens, went through a pair of telescopes to adjust the beam-diameter for EOM switching, and sent into Bob's detection box.

The 532 nm and 1064 nm signals were separated with a second dichroic mirror (DM2). The 1064 nm signal was reflected by the DM2, focused by a $f = 40$ cm lens, and detected by a photodiode. The 532 nm signal passed through both DMs, then went through a 532 nm bandpass filter, reflected by a silver mirror and finally collected by the silicon tracking CCD camera. Since silicon cameras are very sensitive to near infrared signals, the 532 nm filter was placed to filter out the strong 808 nm light during the channel monitoring.

Inside the Bob's detection box, the quantum signal went through a pair of HWP and QWP, which defines the polarization measurement basis, and then incident on a 1-inch PBS. Two $f = 50$ mm lenses were placed at each output of the PBS, to focus the photons onto two free-space coupled single photon detectors. Here 8 nm filter was used in front of each of the detector to filter out the stray light. A picture of the setup built up out of the Coude path

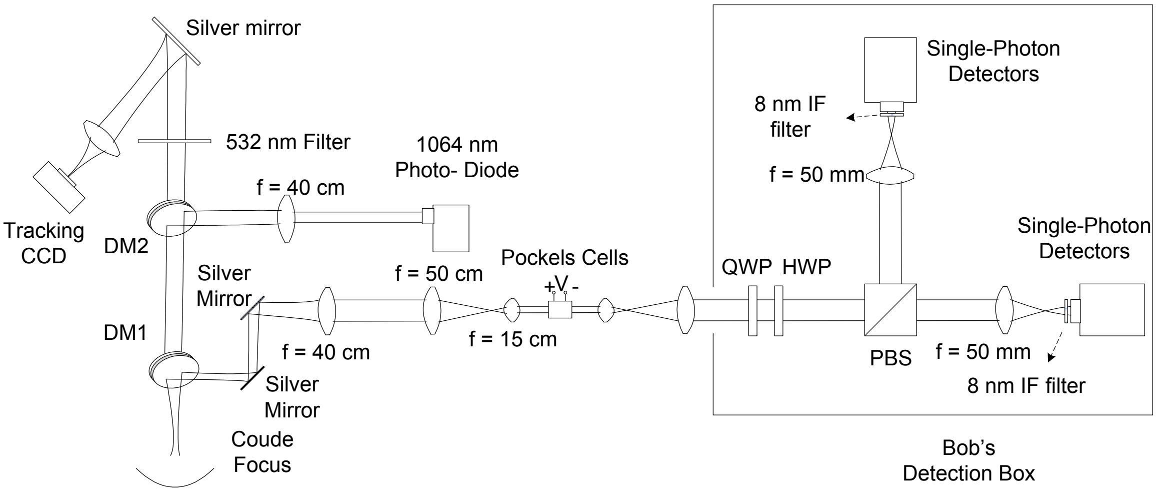

Figure 2.13: Schematic description of the receiver's setup in Tenerife.

of the OGS telescope is shown in Fig.2.14.

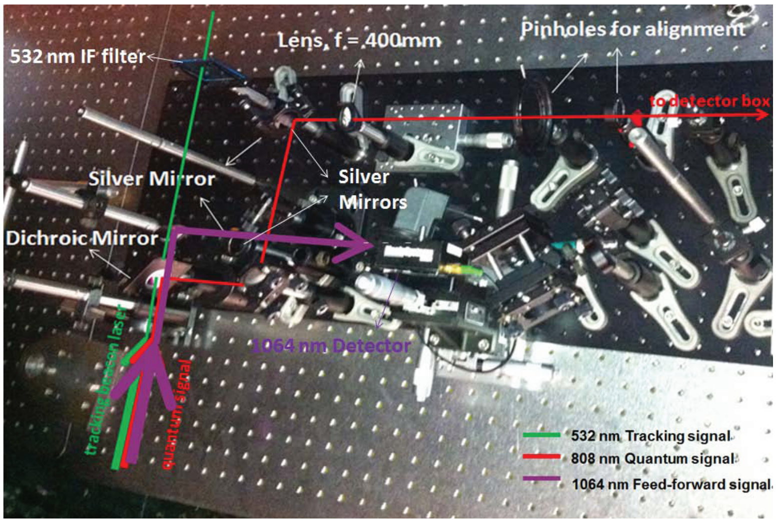

Figure 2.14: A picture of the actual receiver setup deployed out of the Coude path of the OGS telescope. Picture taken by the co-authors of [28].

Chapter 3

Key techniques

3.1 Tracking

In order to stabilize the pointing of the transmitter and receiver telescopes under atmospheric turbulence, we built up a bi-directional closed-loop tracking system on the two sites. The transmitter telescope's platform was actively locked to a 532 nm beacon laser pointing from Tenerife to La Palma and imaged onto a CCD camera. Similarly, the OGS receiver telescope adjusted its pointing direction based on a 532 nm beacon laser attached to the transmitter telescope. A picture of the tracking laser shining out of the La Palma laboratory is shown in Fig.3.1. In every step the tracking system detects and corrects the drift of the pointing direction, thus the long-term drifts in one direction can be avoided. We can see the trace of the tracking spot on the OGS tracking camera in Fig.3.2. Even though this system cannot compensate for fast atmospheric fluctuations, it still enabled a stable optical link for the whole measurement nights.

Figure 3.1: A picture of the tracking laser sent out from the laboratory in Jacobus Kapteyn Telescope at La Palma, taken by the co-authors of [28].

The link attenuation with this tracking system was measured every night, using a strong 808 nm laser shooting from La Palma. In good nights, the link exhibited a total attenuation of 28 dB, from which 3 dB were introduced by the receiver's setup. In such nights, the seeing of the received beacon laser at the OGS was measured to be around 3 arcseconds. The strongest attenuation that still allows our measurements was around 40 dB.

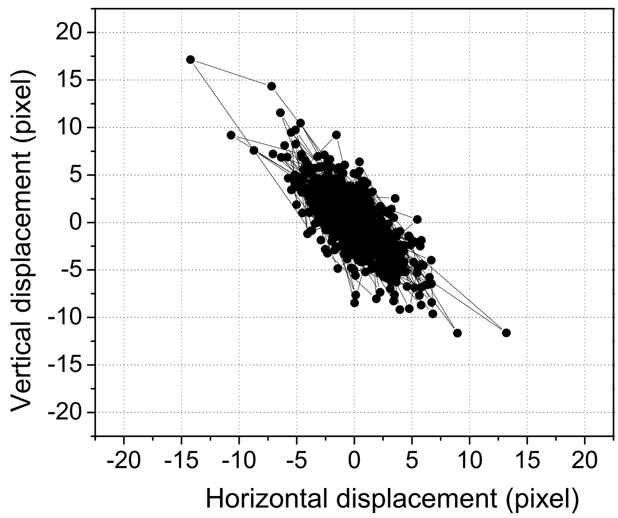

Figure 3.2: Trace of the tracking point on the OGS tracking camera at Tenerife over 100 minutes. We can find the long-term drifts in one direction can be successfully avoided with the tracking. The pixel size of the CCD camera is 4.5 μm.

3.2 Implementation of feed-forward

In the teleportation protocol, the aim of feed-forward is to faithfully transfer Alice's BSM results to Bob. Experimentally, the word "faithfully" would corresponds to two main requirements on the operating the feed-forward system. First, the system should have tolerable error rate and high transmission rate over the high-loss channel. Secondly, the encoding and decoding processes should be considerably fast, since the quantum signal was delayed with the optical fiber, which exhibits unwanted transmission losses per unit length.

Before the final experiments on the Canaries, we designed different coding schemes and tested them on a 10 km free-space link set up between our institute and Kahlenberg in Vienna. In the following sections we will talk about the details of these tests.

3.2.1 Coding methods

We developed in total three coding schemes, as shown in Fig.3.3.

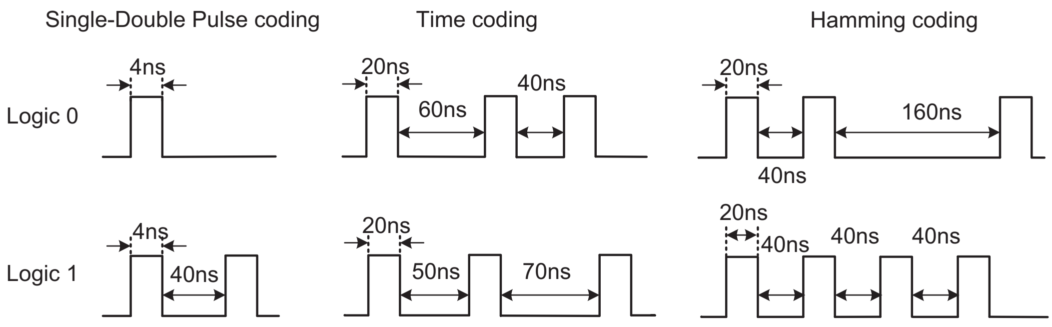

Figure 3.3: Coding schemes.

The simplest coding method is the “single-double-pulse coding”, where logic “0” is encoded as a single pulse, with a pulse duration of 4 ns. Logic “1” is encoded as two successive pulses, each with 4 ns pulse duration, and separated with an interval of 40 ns. The second scheme is called time coding. It encodes the information on the time separation between successive pulses. For example, logic “0” is encoded as three pulses, with time separation of 60 ns between the first and the second pulses, and 40 ns between the second and the third pulses. The last one is the error-correcting Hamming coding, in which logic “0” is encoded as bit series “11001”, and logic “1” as bit series “11110”.

During the first tests, we found that in single-double-pulse coding, the channel loss can result in bit-flip errors if the two pulses experienced different losses during propagation. For example, if one pulse inside logic “1” is too weak to be discriminated, the other stronger pulse would trigger a logic “0” event in decoding. To address this problem, we made a modification to the decoding process, which we call double-threshold discrimination decoding. When a pulse is discriminated with a threshold (threshold 1) pre-set with the constant-fraction-discriminator (CFD), another lower threshold (threshold 2) will be set to check the existence of a second pulse, as expressed with an oscilloscope screenshot in Fig.3.4. This method can avoid the mis-detection of one pulse in logic “1”.

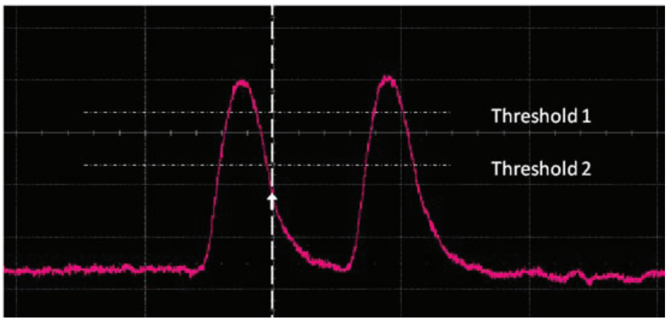

Figure 3.4: Oscilloscope screenshot of the detected signal of logic “1” by a photodiode in single-double-pulse coding. A description of the double-threshold discrimination is sketched.

3.2.2 Proof tests in Vienna

A 10 km free-space link was built up, to test the applicability of the coding schemes. The link is consisting of a set of sender and receiver modules in the institute building, and a retro-reflector on the Kahlenberg in the north of the city. See Fig.3.5. The link is about 10 km round-trip, yields a loss of 42 dB in good weather conditions.

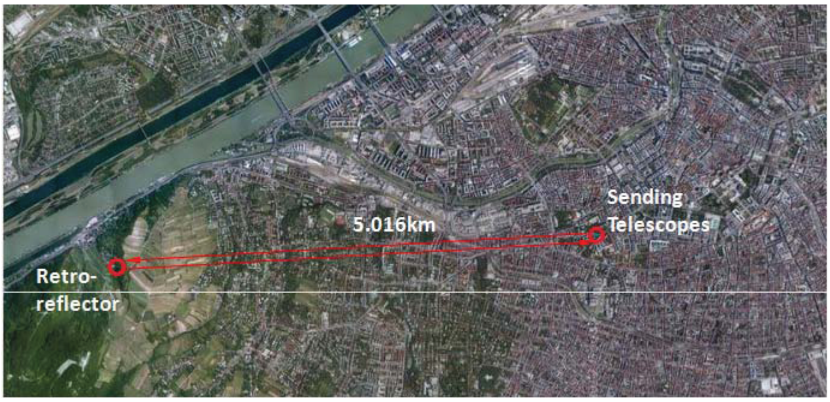

Figure 3.5: A 10 km (round-trip) free-space link in Vienna.

During the test, we triggered the encoder with TTL pulses of 1 kHz repetition rate. The encoded signal then triggered the laserdiodes to emit laser pulses. The emitted light was sent out via three sending telescopes, and then reflected by the retro-reflector, collected by a receiving lens and detected by a Menlo system FPD510 photodiode. A time-tagging-unit (TTU) was used to record the decoded signal. The final results are summarized in Tab.3.1.

Table 3.1: Testing results of the four coding methods. Here “Dbl. Pl. 1 (2)” stands for single-double-pulse coding with single (double) discrimination threshold(s). “Commu. Eff.” represents the communication efficiency of the coding schemes. “Pl. Length” means the length of the electronic triggering signal. “El. Delay” stands for the total delay for encoding, detection, and decoding.

Coding Methods	Error rate		Commu. Eff.		Pl. Length(ns)		El. Delay(ns)		Jitter (ns)
	“0”	“1”	“0”	“1”	“0”	“1”	“0”	“1”	
Dbl. Pl. 1	0%	0.105%	99.97%	99.53%	4	48	103.20	100.80	8
Dbl. Pl. 2	0%	0%	100%	99.997%	4	48	133.15	136.35	8
Time	0%	0%	99.14%	98.94%	160	180	228.90	231.25	30
Hamming	0%	0%	100%	100%	260	200	321.20	322.20	16

We can find that all the four schemes exhibited quite high transmission rate (> 99%) and low error rate (< 0.2%) on this 10 km channel. Considering the complexity and timing budget, we decided to use the double-threshold discriminated single-double-pulse coding in the final experiment.

However, when the same feed-forward setup runs on the 143 km channel, we found that the signal to noise ratio (SNR) we managed to obtain was much lower than in the Vienna test. Then we turned to a most simple coding scheme. That is, when Alice detects a $|\psi^-\rangle$ in her BSM setup, she does nothing on the feed-forward channel. Since Bob will also detect nothing, he keeps his Pockels cells off. If Alice detects a $|\psi^+\rangle$ in her BSM setup, she sends out one pulse on the classical channel. On detecting this pulse, Bob applies a voltage on his Pockels cells, to perform a σ_z operation on the quantum signal. This coding scheme was working with an average efficiency of 23% in the final experiment.

3.2.3 Delay finding

As we talked in Sec.2.5, the single photons were delayed with a 50 m fiber in La Palma to leave sufficient time for Bob to perform the unitary transformation. It's then important to know, at Tenerife, how long the the incoming of single photons was delayed with respect to their corresponding feed-forward pulses. This can be done by cross correlating Bob's two sets of time-taggers, i.e., the time-taggers of the single-photon detection events, and of the feed-forward pulse detection events. We shifted one set of the time-taggers with respect to the other set, and recorded their number of coincidences. Once the single photon detection events are shift to coincide in time with their corresponding feed-forward pulses, we can find a coincidence peak. The time shift Δt where the coincidence peak appears gives the delay.

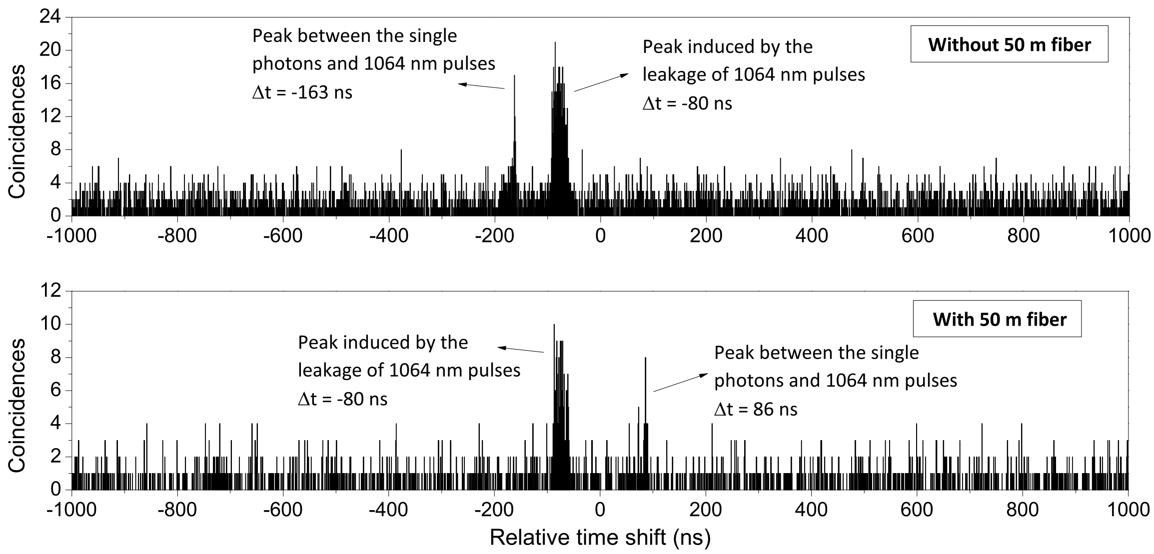

Figure 3.6: Coincidences between the feed-forward pulses and the single photons. The graph on top is from the measurement without the 50 m fiber. The graph downside is from the measurement after the 50 m fiber was plugged in.

Fig.3.6 shows the number of coincidences (y-axis) of the two sets of time taggers, with respect to their relative time shift (x-axis). Surprisingly, we found two peaks in both graphs, which was not in accordance with our expectation. A wider peak is sitting at $\Delta t = -80$ ns in both pictures, and a narrower peak is shifted from $\Delta t = -163$ ns to $\Delta t = 86$ ns with the adding of the fiber. Later analysis showed that the wider peak is introduced by the photons from the 1064 nm feed-forward pulses, which were not fully filtered by the dichroic mirrors. These 1064 nm photons also clicked the single-photon detectors and generated unwanted coincidences. The narrower peak is the actual peak we are searching for, the peak between the single photons and feed-forward pulses, which shifted for 249 ns because of the plug-in of the fiber. The position of the peak $\Delta t = 86$ ns in the lower graph indicates that the single photon is coming 86 ns later than its feed-forward pulse after plug in the fiber.

The loss due to the insertion of the 50 m fiber can be evaluated with the peak value of two-fold coincidences between the single counts in La Palma and Tenerife. Fig.3.7 shows the reduction of the peak two-fold coincidences before and after plug in the 50 m fiber. Before plug in the fiber, as shown in the upper graph, we have a peak coincidence value of 172. The values reduced to 99 after plug in the fiber. Shown in the lower graph. This corresponds to an attenuation of 2.4 dB, means around 42% of single photons was lost.

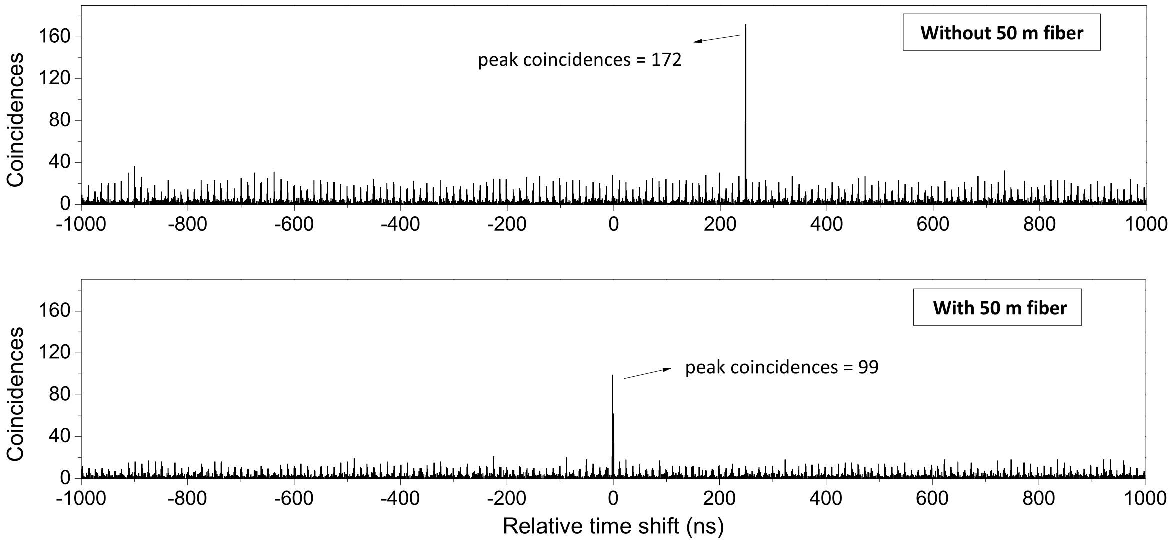

Figure 3.7: Two-fold coincidences between single-photon detection events in La Palma and Tenerife. The reduction of peak value from the upper graph (without the 50 m fiber) and the lower graph (with 50 m fiber) reveals the induced attenuation.

3.3 Detector alignment

In this part we will talk about the alignment of the two single-photon detectors on the receiver's side in presence of the count rate fluctuations. Due to the high channel loss, the raw SNR at the receiver's side is very low. For instance, under 35 dB link attenuation, we can receive about 500 Hz signal counts from La Palma. But the background introduced by the stray light can be up to 2 kHz. The count rate was also fluctuating due to the turbulence. Fig.3.8 shows the count rates of the two detectors over 40 seconds.

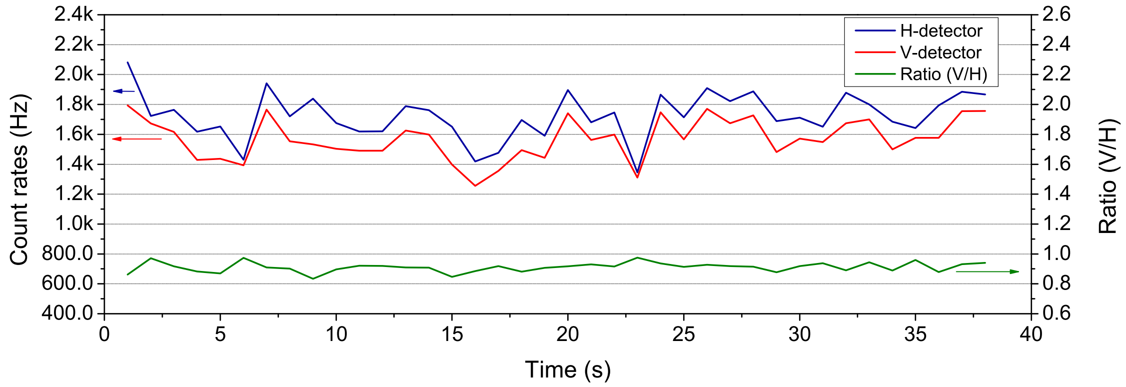

Figure 3.8: Fluctuation of the counts rates of the H- and the V-detector in Tenerife over 40 seconds, when the position of both detectors are fixed. The count rates of each detector are fluctuating but their ratio (green line) remains stable.

Giving the low SNR and fluctuating situations, we normally do the detector alignment in two steps, with a strong 808 nm alignment laser sending from La Palma.

First, we maximize the sending power in La Palma to milli-watt level, such that the spot-dancing on the APD surface at Tenerife is observable with an infrared viewer. Then we move the detector along the focal direction and fix it at the position which gives a smallest spot size. This ensures that the detector is sitting right in the focal range. The horizontal and vertical positions can also be roughly adjusted by observing the reflection strength on the detector surface. As the APD surface is highly-absorptive at 808 nm, and the housing material was selected to be highly-reflective at this wavelength (see Fig.2.6). So if at a position the spot disappears on the detector surface, we can say it's roughly centered onto the APD surface.

The fine alignment of the horizontal and vertical positions is done in the second step. We first reduce the sending power at La Palma to a medium level, which generates around 100 kHz counts on each of the Tenerife detector (we call the alignment light in this procedure "fake singles"). As seen from Fig.3.8, the ratio of the count rates between the two detectors remains stable even if their single rate is fluctuating. So, alignment along the horizontal and vertical directions can be done by observing the ratio between the two count rates. When one detector is moved to the edge of the spot, we will find a dropping edge on the ratio. Then we move the detector backwards to find the dropping edge at the other side of the spot. Finally, we fix the detector at the center positions between the two dropping edges, and this makes sure that it's center to the focal spot.

3.4 Electronics

An overview of design and interconnections of the electronic setup on the two islands is shown in Fig.3.9.

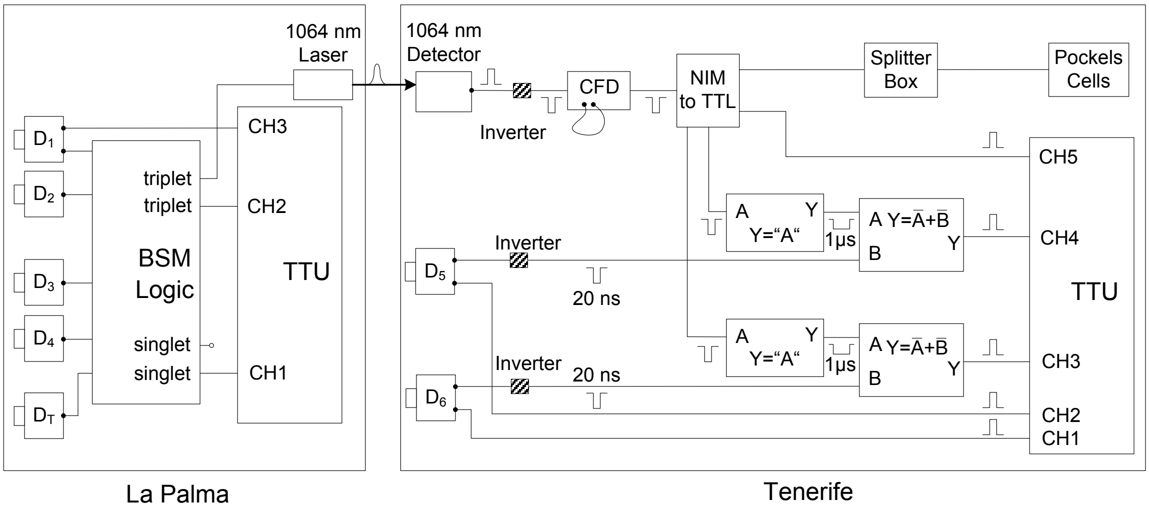

Figure 3.9: Interconnections of the electronics.

At La Palma side, we have five single photon detectors (here we mark the four BSM detectors as D_{1-4}, and the detector of the trigger photon as D_T). Based on a three-fold coincidence event between two of the four BSM detectors and the trigger detector D_T, a logic circuit determines whether a $|\psi^-\rangle$ or $|\psi^+\rangle$ state was observed and consequently features two different outputs that are fed into a time-tagging unit. In case of the $|\psi^+\rangle$ state, a third output triggers the three 1064 nm laser for transmitting this information to Bob. Additionally, a copy of the signal of detector D_1 was directly fed into the time-tagging unit, such that two-fold coincidences between La Palma and Tenerife could be used for the fine synchronization of the individual time bases.

At Tenerife, the 1064 nm laser pulses were detected with a high sensitivity photodiode produced by Menlo systems. Once a pulse is discriminated, a trigger will be sent to the Pockels cells. The duplicate of the single photon detector signals were logically combined (AND gate) with a signal indicating whether the Pockels cells has been on or off. At the end, the "raw" detector signals, the logically combined signals and the classical trigger signal were fed into the time tagging unit at Bob.

Chapter 4

Measurement results

4.1 Local performance of the teleportation setup

Before the final inter-island experiment, the local performance of the teleportation setup was evaluated at La Palma. The results are summarized in Tab.4.1.

Table 4.1: Local performance of the teleportation setup.

EPR rate	Fock-source rate	4-fold count rate local	4-fold count rate expected at 30dB	Entanglement visibility local	Teleportation fidelity local
180.000 counts/s	140.000 counts/s	180 counts/s	0.18 counts/s	88%	89%

The local performance measurements were repeated before every measurement night and the setup was realigned to yield these values when necessary.

4.2 Measurement results of the inter-island experiment

In the inter-island experiments, we teleported a total of 5 states (e.g. H, V, P, L and R), which is sufficient to conclusively demonstrate quantum teleportation while minimizing the required integration time. In the first stage, we teleported the four input states (H, V, P ,L) without real-time feed-forward, and performed tomographic measurements in three consecutive nights. For these measurements, we accumulated data over 6.5 hours with 605 four-fold coincidence counts, which corresponds to an average free-space link attenuation of 35 dB. Late wards, two states (P ,R) were teleported with feed-forward in the following nights.

Fig.4.1 shows the state tomography results of quantum teleportation. The measured density

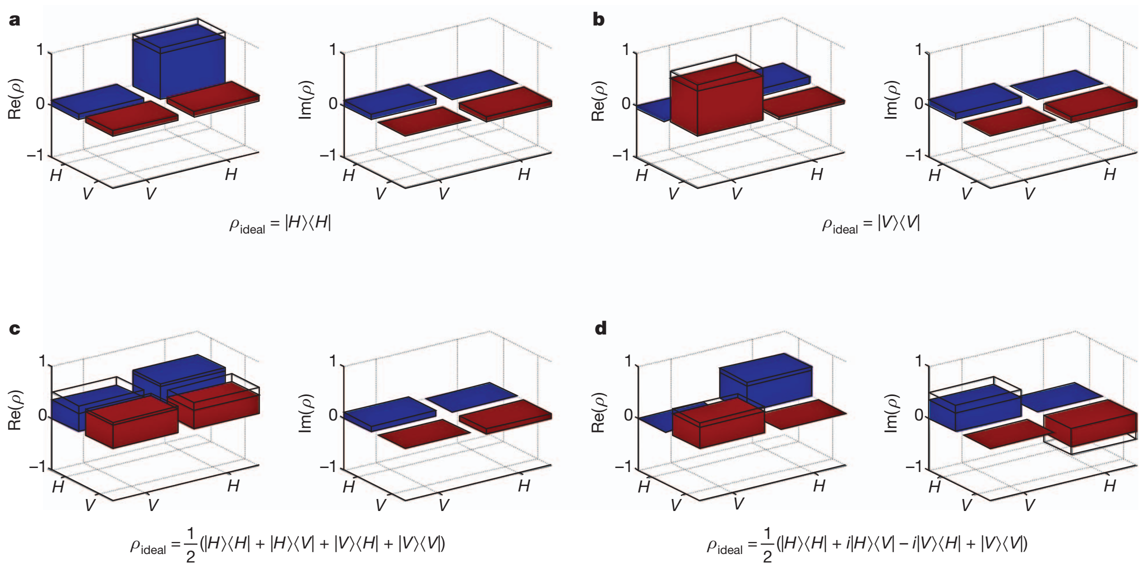

Figure 4.1: State tomography results (without feed-forward operations) of the four quantum states over the 143 km free-space channel. The bar graphs show the reconstructed density matrices ρ for the four states teleported from Alice (La Palma) to Bob (Tenerife). The wire grids indicate the expected values for the ideal cases. The data shown comprise a total of 605 four-fold coincidence counts in about 6.5 hours. The uncertainties in state fidelities extracted from these density matrices are calculated using a Monte-Carlo routine assuming Poissonian error. Picture taken from [28].

matrix ρ for each of these teleported states was reconstructed from the experimental data using the maximum-likelihood technique [38]. The fidelity of the teleported state is defined as the overlap of the ideal teleported state with the measured density matrix. For this set of states, the teleported state fidelities were measured to be

- H with $f = 0.890(42)$;
- V with $f = 0.865(46)$;
- P=H+V with $f = 0.845(27)$;
- L=H-iV with $f = 0.852(37)$;
- P_f=H+V with $f = 0.760(50)$;
- R_f=H+iV with $f = 0.800(37)$

Despite such high loss in the free-space channel, the classical average fidelity limit [10] of 2/3 was clearly surpassed by our observed fidelities, as shown in Fig.4.2.

Moreover, the reconstructed density matrices of the teleported quantum states allow us to fully characterize the teleportation procedure by quantum process tomography. The four input states (H, V, P, L) and their corresponding (reconstructed) output states are used

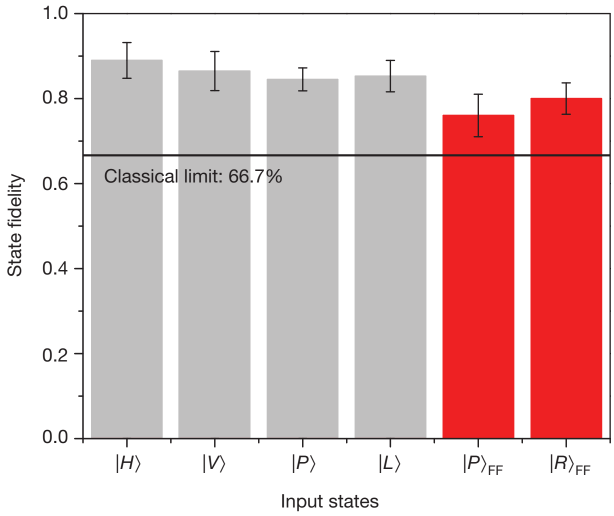

Figure 4.2: State fidelity results for the four unbiased-basis states teleported from La Palma to Tenerife. Error bars are given by Poissonian statistics. Picture taken from [28].

to compute analytically the process matrix of quantum teleportation. We can completely describe the effect of teleportation on an input state ρ in by determining the process matrix χ, defined by $\rho = \sum_{l,k=0}^{3} \chi_{lk}\sigma_l \rho in \sigma_k$, where the σ_l (σ_k) are the Pauli matrices with σ_0 the identity operator. The process fidelity we get is $f_{process} = 0.710(42)$. See Fig.4.3. This clearly confirmed the quantum nature of our teleportation experiment as it is 5 standard deviations above the maximum process fidelity of 0.5, which is the limit one can reach with a classical strategy where Alice and Bob do not share any entanglement as a resource.

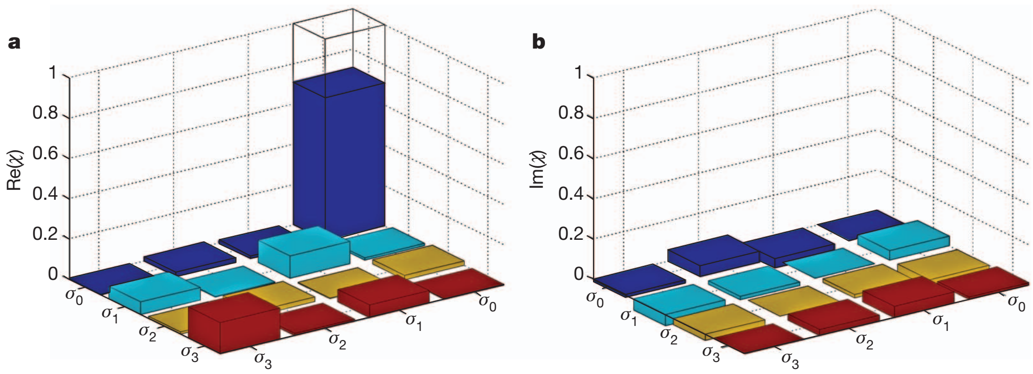

Figure 4.3: The real-part and the imaginary-part **a** and **b** of the reconstructed quantum process matrix. As expected, the dominant component of σ_0 is the contribution of the identity operation, yielding an overall process fidelity $f_{process} = 0.710(42)$. Picture taken from [28].

Part of the results presented in this chapter were taken from the co-authored paper [28].

Chapter 5

Signal analysis

In long distance quantum optical experiments, the geometrical separation makes it unfeasible to identify coincidences between separated sites at real-time. Normally the data is first recorded locally at different sites. A server is used to gather the data and search for coincidences by post processing. Also, as a perquisite for the coincidence searching, one has to set up a common clock among the data recorded at separated sites. In this chapter we will talk about the methods and techniques we used for data recording, processing and synchronization.

5.1 Data recording

On each island, we used a time-tagging unit (TTU) programmed from a field programmable gate array (FPGA) board to write the experimental data. The TTU has 8 input channels. Each set of signal was fed into one of the channel in terms of TTL pulses. On detecting the rising edge of a TTL pulse, the TTU writes down the time (time-tagger) according to a local clock, and the serial number of the input channel. Each time-tagger is consisting of 16 bytes. The first 8 bytes indicate the input channel (channel 1 to channel 8). The following 8 bytes record the time of the event, with a step size of 156.25 ps. The format of the time-taggers is shown in Fig.5.1.

```
    Input channel                                   Time information
00 00 00 00 00 00 1C 40   00 00 00 00 20 1F 57 41
00 00 00 00 00 00 00 40   00 00 00 00 32 ED 5B 41
00 00 00 00 00 00 00 00   00 00 00 40 64 CD 6E 41
00 00 00 00 00 00 F0 3F   00 00 00 A0 A9 A8 61 41
00 00 00 00 00 00 1C 40   00 00 00 00 20 C9 64 41
```

Figure 5.1: Format of the time-taggers. Each time-tagger is consisting of 16 bytes.

The final aim of data processing is to identify the four-fold coincidence between the time-tagger sets generated at La Palma and at Tenerife, which confirms a successful teleportation event. Accordingly, at La Palma, we recorded the three-fold coincidences between the two-fold BSM outputs ($|\psi^-\rangle$, $|\psi^+\rangle$) and the detection events of the trigger photons. At Tenerife, we recorded the detection events of the two single-photon detectors, and the detection events of the 1064 nm pulses in feed-forward measurements. Additionally, for synchronization purposes, we recorded the detection events of a single detector in the BSM setup at La Palma, for identifying the two-fold coincidences. The recorded data sets are listed in Tab.5.1.

Table 5.1: Data recording in La Palma and Tenerife. Here GPS 1PPS pulses refers to the one-pulse per second (1PPS) signal from the Global Positioning System (GPS) clock module, which were used in the coarse synchronization of the clock.

La Palma		Tenerife	
CH1	$|\psi^-\rangle$ AND trigger photon	CH1	H-detector
CH2	$|\psi^+\rangle$ AND trigger photon	CH2	V-detector
CH3	Single photon detector in BSM	CH3	CH1 AND CH5
CH4	—	CH4	CH2 AND CH5
CH5	—	CH5	Feed-forward pulses
CH6	GPS 1PPS pulses	CH6	GPS 1PPS pulses

A server was set up in La Palma to start and stop the data recording. On starting of the measurement, the server starts to write the local measurement data, and at the same time sends out a starting order to Tenerife. Note that, due to the unavoidable network transmission time, the writing of the two time-tagger sets will not be started at the same time, i.e., there is an time offset between the first Alice time-tagger and the first Bob time-tagger. This offset will be calibrated during the coincidence searching process with the GPS 1PPS signals.

5.2 Data flow

As we already talked about in the previous section, the experimental data was first recorded locally at the two sites, labeled with the number of measurement rounds. Each measurement round was set within 40 s to 180 s to avoid the long-term GPS clock drift (detailed in Sec.5.4.1). After each round, the data at Tenerife was transferred to the La Palma server via network stream. A *c++* coincidence searching program was running on the La Palma sever to analyze the coincidences between the Tenerife file and the La Palma file collected within one measurement round. The output of this *c++* program is a coincidence matrix in form of comma-separated value (CSV) file. The CSV files from different measurement rounds were then collected by a Labview program, to finally analyze the total number of coincidences. The key parameters, such as the teleportation visibility, fidelity, etc., were calculated out from the results of the Labview program. Fig.5.2 shows the overall data flow of the experiment.

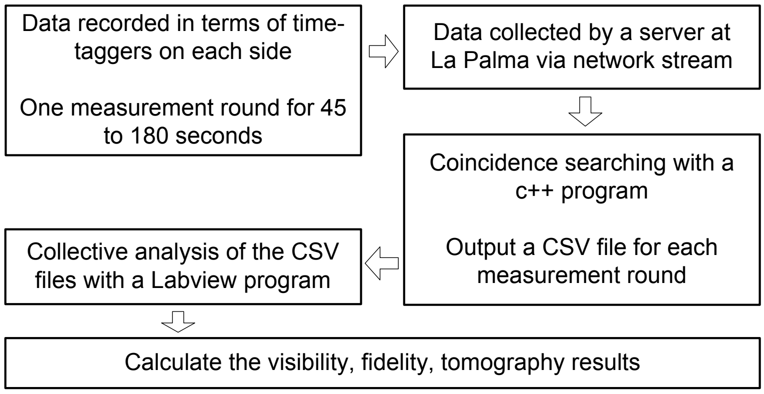

Figure 5.2: Flow of data processing.

5.3 Coincidence searching

Coincidence searching acts as a key procedure in the data processing. A coincidence event is confirmed when two or more events take place within a coincidence time window. In our teleportation experiment, a successful teleportation event is confirmed by a four-fold coincidence event, among the receiver's photon detection event in Tenerife, the detection of the two BSM input photons and the trigger photon in La Palma.

A coincidence searching program was used to identify the coincidences between the two sets of files. Here we give a brief introduction of the coincidence finding process. In the following discussions, we refer to the variables as shown in Tab.5.2.

Table 5.2: Variables in the coincidence searching program.

achan	input channel of Alice's time-tagger
bchan	input channel of Bob's time-tagger
atime	time-tagger of Alice's event
btime	time-tagger of Bob's event
offset	time offset between Alice's and Bob's first 1PPS signal
laufzeit	photon flying time from La Palma to Tenerife
histwid	half width of the coincidence window
binzahl	number of bins in the range of calculation
timetagunit	bin size of the time-taggers, 156.25 ps in our case
outputperiode	range of output, defined with number of 1PPS pulses
gpscycle	number of processed GPS 1PPS pulses

The program is working as follows:

1. Find the first 1PPS tagger in Bob's file (Channel==6)

2. Find the first 1PPS tagger in Alice's file (Channel==6)

3. *offset*=*btime*-*atimecycle*[0]+*laufzeit*, calculate the offset between the two starting time tagger

4. If *offset*>*gpstolerance* or *offset*< −*gpstolerance*, which means Alice and Bob were not started with the same 1PPS signal. Then find next Alice/Bob 1PPS tagger

5. Find next Bob tagger at *btime*

6. Calculate *diff*=*btime* − *atime*−*offset*, the time difference between current Alice's and Bob's taggers

7. Find next Alice time tagger till *btime*, search if any Alice time tagger satisfies *diff*< *histwid*. If yes, coincidence event confirmed, add to the array of coincidences

8. Continue find next Bob tagger and redo the search of Alice tagger as in step 7

9. Repeat step 8, scan over the file within the input gpscycle

10. Make tables and write output files

Fig. 31 shows the coincidence peaks calculated by the coincidence searching program. The central peak has a width of about 5 ns, corresponds to a 2.5 ns coincidence window. In the final analysis of the experimental data, the coincidence window was set within 2 to 3 ns.

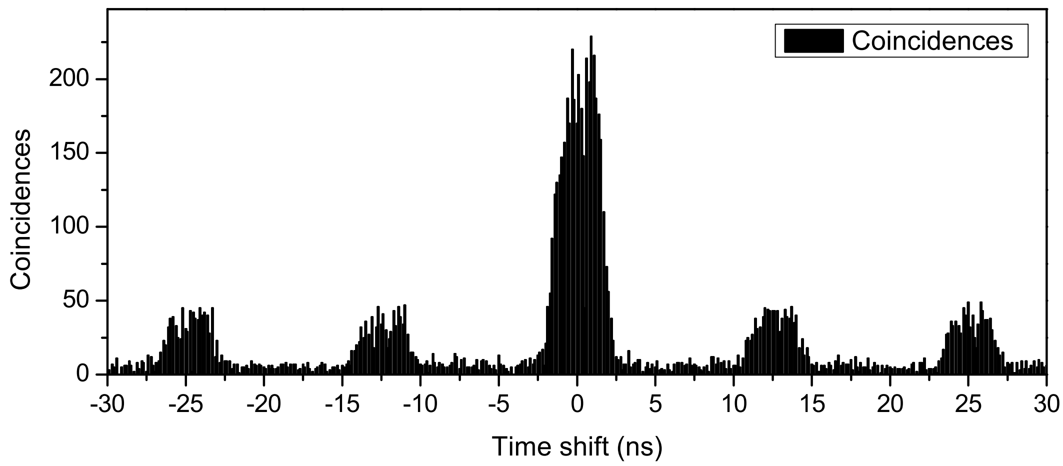

Figure 5.3: Coincidence peaks generated with the coincidence searching program. The central peaks refers to the "signal" coincidence peak, i.e., generated by the photons in the same down-convertion pair. The side peaks were generated by photons coming from different UV pulses, we refer them to "noise" peaks.

5.4 Clock synchronization

In long-distance optical experiments, synchronization is usually done by sending strong laser pulses with a defined repetition rate from site to site. This enables timing accuracy down to 1 ns but requires to set up additional optical channels. In our experiments, we found out that the weak quantum optical signal, the entangled photon pairs generated with pulsed laser pumping, are potentially a good resource for synchronization. Following this idea, we synchronized the teleportation events (four-photon coincidences) with two-photon coincidences. This method gave accuracy of 2 ns, and worked at up to 40 dB attenuation. We also think that, the applicability of this method may not only be restricted in photonic experiments. In principle, it can be employed in any distributed experiments wherever a quantum optical link (fiber or free-space) can be setup.

5.4.1 Limitations on timing accuracy

Experimentally there are several limitation factors on the accuracy of our synchronization method. For instance, the jitter of the photon detectors, the jitter of electronic devices, the quantum limit of joint bi-photon detection, and so on. In our setup, the local clocks were phase-locked with the 10 MHz clock from the GPS module (details in Sec.5.4.2). The GPS clock can drift up to 20 ns over long measurement time [23]. But this can be avoided by switching to many shorter measurement runs (45 to 180 seconds), this can reduce the drift down to 1 to 2 ns per measurement run. Our single photon detectors have around 500 ps timing-jitter, and the electronics is giving a jitter less than 1 ns. The quantum limit of the bi-photon detection would not be comparable with the electronic noises, since we were using an ultrafast pump laser with 140 fs pulse duration. So, considering all these effects, we would be able to get a timing accuracy down to 2 ns.

5.4.2 GPS clock

Before the fine synchronization with photons, the two time bases were first coarse synchronized with the Thunderbolt® GPS Disciplined Clock modules. The module disciplines the 1PPS signal from the GPS satellites with a local 10 MHz oscillator, and outputs the disciplined 1PPS signal. On each island, the disciplined 1PPS pulses we fed into the TTU. As stated in the manual, the synchronization accuracy with the GPS modules between difference sites is around 10-15 ns.

5.4.3 Synchronization based on two-fold coincidences

After the coarse synchronization, fine timing can be done with the two-fold coincidences between the two time-tagging sets of single photon detection events (one set from the single detector in the BSM setup at La Palma, another set from one of the detectors in Tenerife). The two-fold coincidence peak between these two sets yields the precise timing position where the four-fold coincidence peak should appear, as shown in Fig.5.5. This procedure was

Figure 5.4: Thunderbolt® E GPS Disciplined Clock. The disciplined 1PPS pulses can provide synchronization between separated sites, with accuracy between 10 to 15 ns. Picture taken from http://www.trimble.com.

performed every 45 to 180 seconds and allowed to precisely synchronize the individual time bases at Alice and Bob.

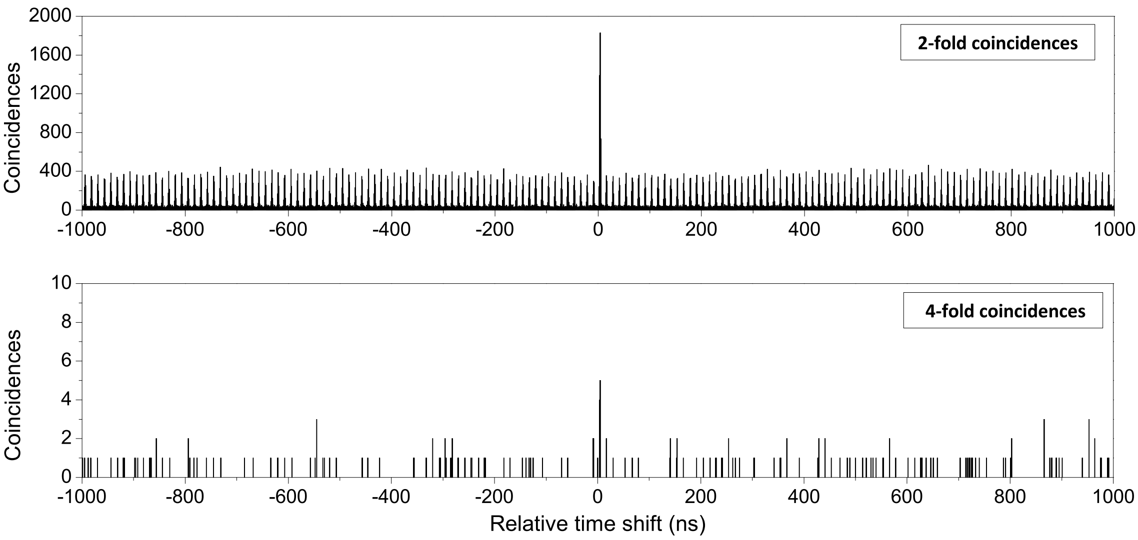

Figure 5.5: The upper graph shows the two-fold coincidence peak, which indicates the precise shift between the individual time bases at La Palma and Tenerife. The lower graph shows the corresponding four-fold peak at the very same time position.

5.5 SNR and coincidence window size

Coincidence searching is essentially a temporal filtering process. Theoretically, a narrower coincidence window corresponds to a stronger temporal filter and would give a higher SNR (visibility in our experiment). However, experimentally the size of coincidence window is limited by varies factors. e.g., the jitter of electronics, the accuracy of the clock synchronization, the signal instability induced by the link turbulence. In presence of these factors, if the coincidence window is set too narrow, parts of the signal counts may be wiped out. This results in a stronger loss of signal counts. On the other hand, if the coincidence window is set too wide, the probability of count in a background event is also higher. In both cases the SNR will decrease. Therefore, it is of importance to investigate how the coincidence window size influences the optimal SNR.

We picked up the data from a high attenuation (38 dB) night for the analysis, in order to see more pronounced influences. The results are presented in Fig.5.6. Here we define the background coincidences as the average value of the ten highest side-peak values, and the SNR as the ratio of peak coincidences (signal) to background coincidences (noise).

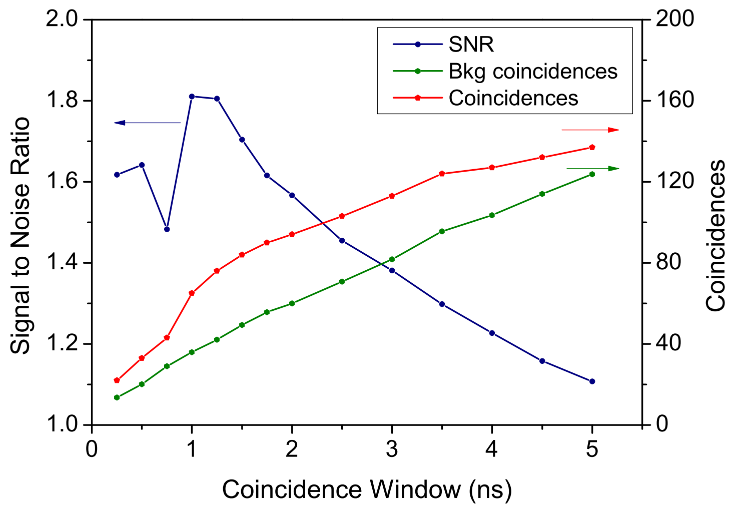

Figure 5.6: SNR with respect to the size of coincidence window. Here the red line "coincidences" stands for the value of central coincidence peak (signal), and the green line "Bkg coincidences" represents the background coincidences (noise). The blue line "SNR" means the ratio of signal to noise.

As seen from Fig.5.6, the background coincidences are increasing linearly with the coincidence window size. This is in accordance with the assumption of random noise distribution. Within the range of 1 to 3.5 ns, the peak coincidence increases faster than the linearly increased background. An optimal range of coincidence window was found out at around 1.0 to 1.5 ns, which gives the highest SNR. Together with the consideration of the total number of counts, which determines the size of error bars, we applied the coincidence window as 2 to 3 ns in the final analysis.

5.6 Scintillation

Scintillation is introduced by the fast local variations of refractive index in the atmosphere, led by the small-scale temperature gradients. The induced interference effect by scintillation can have a great influence on the link efficiency, and moreover, at millisecond time scale which was not real-timely visible in our experiment. Since the count rates of our detectors were sampled every second, the fast variations were averaged out.

The effects of scintillation on the single photon transmission can be made visible with short interval sampling on the time-tagging files. As shown in Fig.5.7, we sampled the counts of our two receiver's detectors every 50 ms, over a 6 s period.

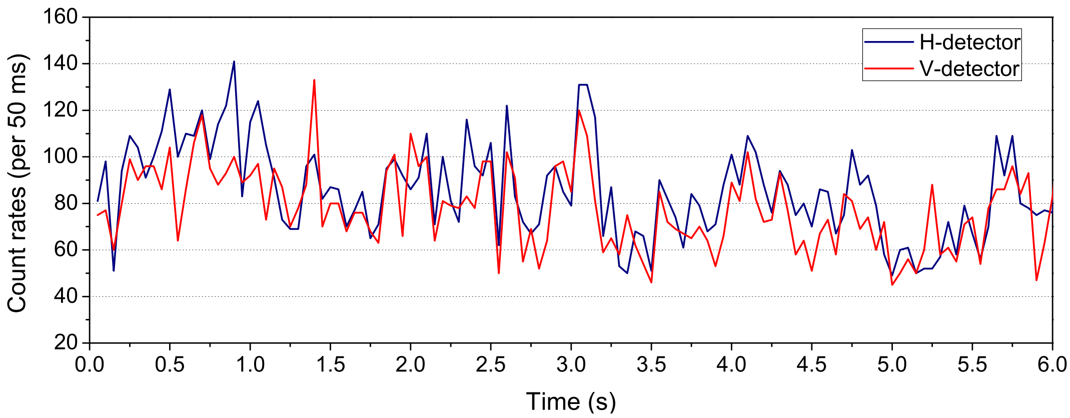

Figure 5.7: Count rates of the two Tenerife detectors over 6 s time interval. Sampled every 50 ms. Here, we can clearly see the fast fluctuations introduced by the scintillation.

The fast fluctuations are clearly shown in the figure, with the count rates varies from 45 to 140 per 45 ms. To see the statistics, we made a histogram for the probability of occurrences of the two detectors' count rates in Fig.5.8. The blue bars represent the H-detector, and the red bars represent the V-detector.

If we assume the distribution of the count rates follows Gaussian statistics, we can further fit their probability of occurrence p_H, p_V as

$$\begin{aligned} p_H &\approx \frac{1}{38.93 \times \sqrt{\pi/2}} e^{-2(\frac{C-85.08}{38.93})^2}, \\ p_V &\approx \frac{1}{34.66 \times \sqrt{\pi/2}} e^{-2(\frac{C-78.88}{34.86})^2}. \end{aligned} \tag{5.1}$$

The H-detector has an average count rate of 85.08 per 50 ms (1701.6 Hz), and the V-detector has slightly lower average count rate of 78.38 per 50 ms (1567.6 Hz).

Scintillation can greatly affect the link efficiency. On the other hand, it also offers a possibility to distill an efficient link out of the fluctuating link.

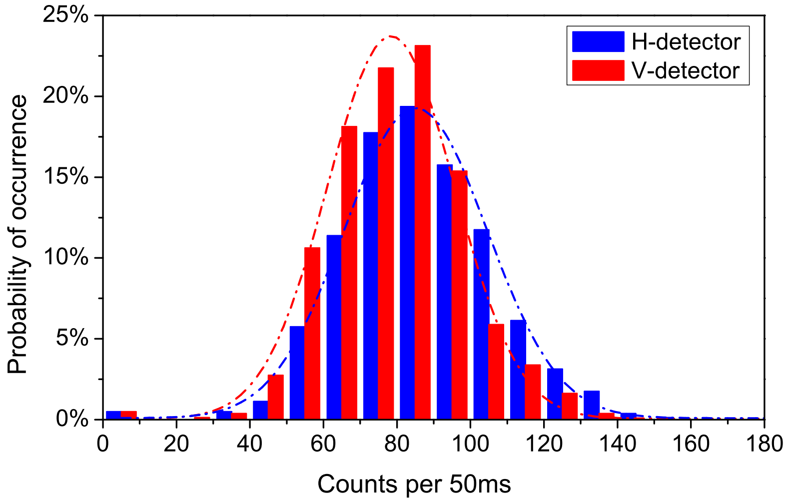

Figure 5.8: Histogram of the probability of occurrences of the two detectors' count rates.

The idea goes as follows. Assuming the fluctuating link gives an average count rates per unit time $\bar{C}$, yields an average SNR of $\bar{r}$. In a short period of time the link efficiency can be higher than average. In this period we will receive more signal photons compared to the background. The average SNR will also be higher than $\bar{r}$. Similarly, in another period of time, the link efficiency can be lower than the average, gives a lower SNR with respect to $\bar{r}$. If the protocol allows one to cut off the data in the period when the count rates (link efficiency) are lower than a threshold, and keep the data in the period when the count rates are higher than the threshold. One can thus get an "effective" link which gives a higher SNR, on sacrificing the total number of counts. For the experiments like quantum key distribution, where losing part of the qubits is not very crucial, this idea can be quite beneficial.

We tried to implement this idea on our teleportation data. The data blocks in the H- and V-channel were cut off when they give a count rate per 50 ms lower than a threshold value. As shown in Fig.5.9, we can see an increasing of four-fold visibility from 75% to 92%. But note that due to the limited data volume (total four-fold coincidences around 120 in the original data), the error bars of the visibility are keeping increasing with the decreasing number of total counts.

5.7 Sunrise

To avoid the influence of sunlight, all our inter-island experiments were performed during night time. It's then an interesting question that to which extent of sun exposure can the experiment still tolerate. During the carrying out of our experiments, the sun rose at around 06:30 local time, in the opposite of the pointing direction of our receiving telescope. We can

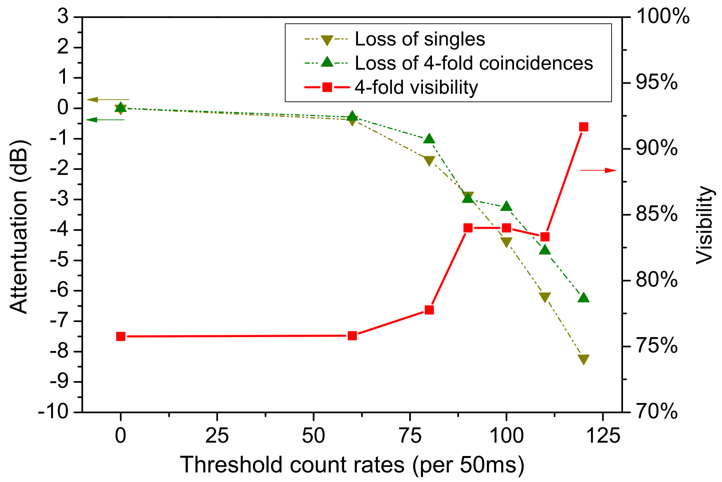

Figure 5.9: With the increase of the threshold count rate up to 120 counts per 50 ms (2400 Hz), the four-fold teleportation visibility increased from 75% to 92%. The loss of counts due to the distillation is expressed in terms of attenuation (dB). Due to the induced attenuation, the total number of effective counts is decreasing with the threshold, results in an growing error bar of the four-fold visibility.

find dramatic increase of the count rates on the receiver's detectors at that time. Normally the experiment was terminated when the count rates increased to 2-4 times higher than in the night.

By post-processing the data, we found that even the single count rates increased up to 2 to 4 times higher, our temporal filtering (coincidence searching) process still keep the noise (background coincidences) at reasonably low level. Fig.5.10 shows the analysis results for the data at sunrise time in the ninth measurement night. We can find the signal and noise coincidences kept at almost same level as in the night, even if the single count rates increased up to 4 times higher. This indicates that we might still be able to perform the measurement after 7 o'clock in the morning.

5.8 Channel statistics at long time scale

In Sec.5.6 we discussed the fast fluctuations of link efficiency at millisecond scale which are introduced by scintillation. Such fluctuations also appear in a slower manner over longer time scale. As shown in the upper graph of Fig.5.11, we plotted the local two-fold coincidence rate at Tenerife (coincidences between the detections of feed-forward pulses and the single photons, give an direct estimation about photon transmission rate) over two hours' measurement time. The data plotted here was sampled with 4 minutes running average, to suppress the fast fluctuations. We can find dips of the signal rates lasting for 10 to 15 minutes. Not like

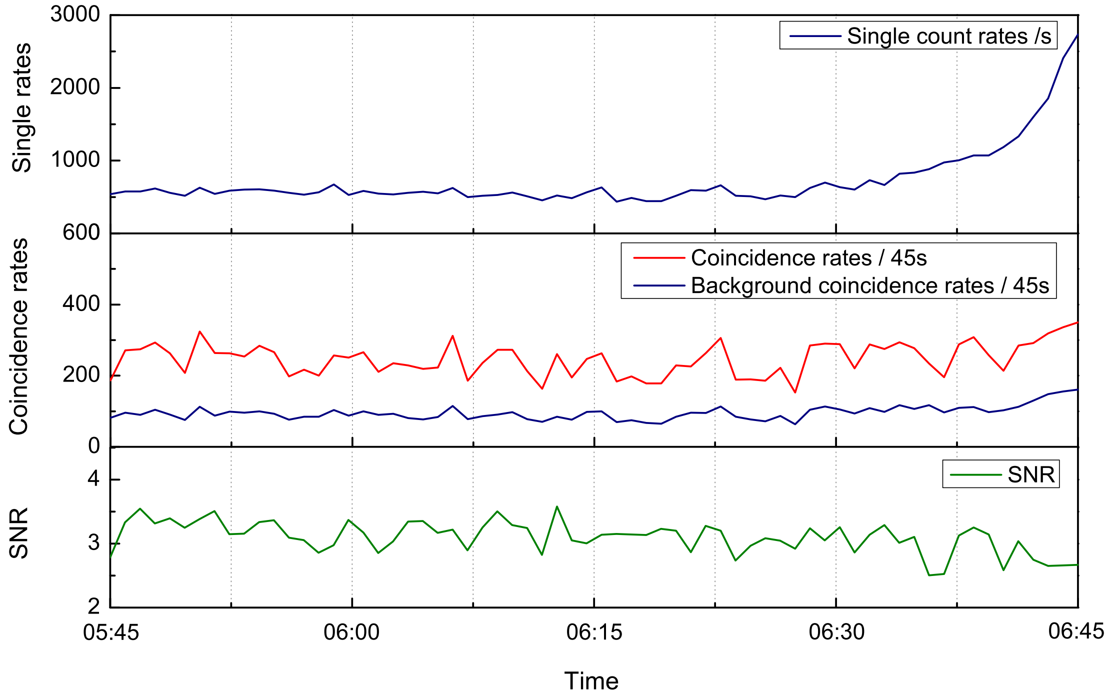

Figure 5.10: Single count rates, coincidences and SNR at sunrise time in the ninth measurement night.

scintillation which is caused by the small-scale fast index variation, this kind of slow variation is most likely introduced by slower atmospherical changes. For example, the wind, clouds, humidity and so on.

To see how the optical properties of the free-space channel varies over long time, we collected the data of the astronomical seeing during this measurement period, shown in the lower graph of Fig.5.11.

The seeing is a parameter used by astronomers to characterize how Earth's atmosphere perturbs the images as seen through a telescope. In astronomical observations, the optical properties of the atmosphere can be characterized with the diameter of a "seeing disc". It can be evaluated by taking a long-exposure (for seconds or even minutes) picture of a star. The different distortions during the imaging period will average out as a filled disc called the "seeing disc". The diameter of the this disk, often defined as the FWHM or the $1/e^2$ diameter, is a common measure of the seeing conditions.

In our experiment, the seeing directly affects the size of the focal spot at the Coude focus, and further influences the collection efficiency of the photon detection modules. In principle, a higher seeing value leads to a larger "angle of arriving". This will cause an expansion of the focal spot on the detector surface, and finally leads to lower detection rates. We can see from Fig.5.11 of a trend of anti-correlation trend between the two curves. The dashed line in the lower graph of Fig.5.11, y=3.731 arcsec., refers to a characteristic seeing value of our 143

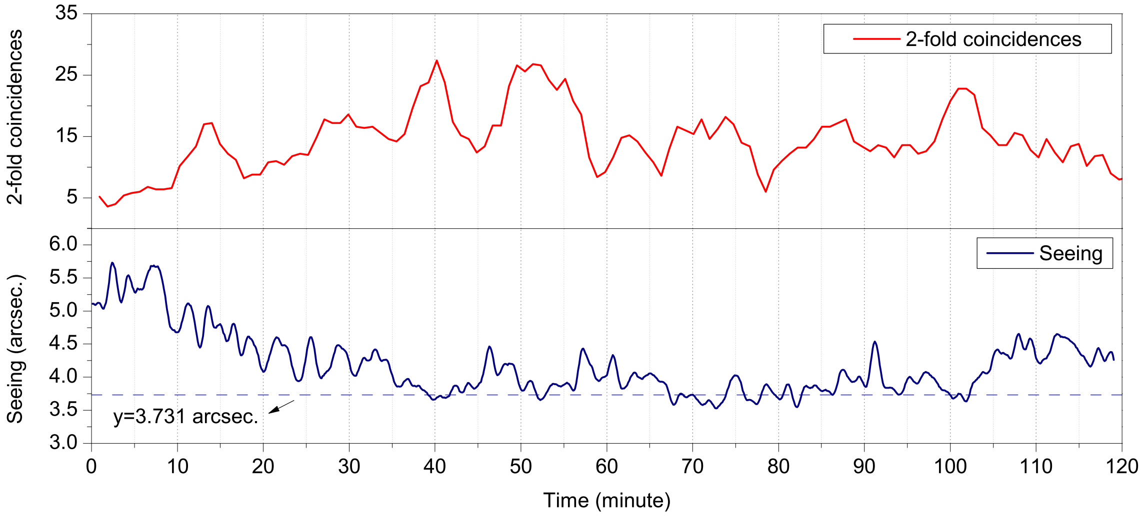

Figure 5.11: The local two-fold coincidence rates in Tenerife, and the seeing data collected by the OGS tracking system at the same measurement time. Sampled with running average of 4 minutes.

km free-space channel, which corresponds to a 338 μm-diameter spot on the detector surface [40].

The seeing is a good measure for the slow variations of the atmosphere, which influences the link efficiency in a slower manner and over longer period of time.

Chapter 6

Conclusion and outlook

In this work, we discuss the details of a recent experiment of quantum teleportation over a 143 km free-space channel. The link was set up in between two Canary Islands, La Palma and Tenerife, gave an attenuation of 28 to 39 dB during the measurement period. We teleported in total 6 states, 2 with and 4 without real-time feed-forward. The fidelity we obtained from all those measurements were clearly surpassing the classical fidelity bound.

To cope with the high-loss channel, we set up a frequency-uncorrelated entangled photon source at La Palma, a set of ultra-low-noise single-photon detectors at Tenerife and a closed-loop tracking system to stabilize the free-space link. On the other hand, we developed a synchronization method with entangled photon pairs, which provided a timing accuracy of 2 ns between the two sites. A set of post signal analysis work was done after the experiment, to give a more comprehensive understanding about the free-space channel, which may provide instructions for our future experiments.

This experiment would represent an important step towards future space-ground quantum communication network. Since our teleportation setup was able to achieve coincidence production rates and fidelities to cope with the link attenuation between a ground-based transmitter and a low-earth-orbiting (LEO) satellite receiver. The technology implemented in this experiment reached the required maturity both for satellite and for long-distance ground communication. We expect that many of the features implemented here will be key blocks for a new area of fascinating experiments.

Acknowledgements

The work presented in this thesis was conducted at the Institute for Quantum Optics and Quantum Information of the Austrian Academy of Sciences. In the first place, I would like to express my sincere thanks to Xiaosong Ma, Rupert Ursin, Thomas Scheidl and Thomas Herbst, for directly supervising me, providing me outstanding guidance and sharing extensive knowledge with me. They also helped me a lot in the daily life on the Canary Islands. I feel grateful to Professor Anton Zeilinger, for offering me the chance to perform the thesis work in his group, and providing suggestions and supervision during the experiment and paper work. Also, I want to thank the administrative and technical stuffs in the institute, Verena Bock, Daniela Charlesworth and Martin Aspöck, they provided me generous help in settling down in Vienna and coping with the daily work in the institute. I also feel very fortunate to work with the photonies in the institute, Marissa Giustina, Alexandra Mech, Amir Tavala, Bernhard Wittmann, Luo Qi, Sven Ramelow and many others.

I must give the best thanks to the personnel at my home university in Jena. To Professor Holger Gies, my supervisor at the home university, who provided me generous and patient help before, and all although the thesis work. To our coordinator Ricarda Knetsch, who gave me numerous guidelines and suggestions in going through all the administrative steps. To Professor Malte C. Kaluza, who helped me in dealing with the Erasmus exchanging. To my student mentor Stefan Flauder, for helping me settling down in Jena and getting use to the Jenaer life, and to Szilvia Mammel for all the reimbursement affairs. Also, I want to thank all the students in the Master of Photonics program, with them we built up the warmest environment in Jena. I wish them all the best with their studies and careers.

I want to thank my family, my parents and brother, for their most warmest supports all the way on my studies, work and daily life, in China and in Europe.

There are still a lot of names I want to thank but not able to all list out here. My thanks for all of you.

Appendix A

C++ codes

A.1 source code: readoutChannels.cpp

```cpp
/**************************************************************
Program to read out the time-taggers from the binary files
by Daqing Wang, May 2012
**************************************************************/

#include <iostream>
#include <fstream>
#include <string>
#include <sstream>

using namespace std;

#define CH1 1
#define CH2 2
#define CH3 3
#define CH4 4
#define CH5 5
#define CH6 6
#define CH7 7
#define BIN_RESOULTION (1 / 6400000000)


unsigned long * readOutFiveChannel(string sourceFileName);
//Function to read out CH1 to CH7 in one binary file, input file name, return 0
string getNextFileName(string FileNameCharacters, string
FileNameCharactersEnd, int FileNameNum);
//Function to get next file name to process

/**************************************************************
main function
**************************************************************/

int main () {
    int numOper, FileNameBeg, FileNameEnd;
    /*the number to control the series reading, starting serial number of the file, ending serial number*/
```

```

of the file
    unsigned long * NumofCounts = NULL;
    //pointer for counting the number of time-taggers
    string currFileName, FileNameChar, FileNameCharEnd, OutputFileNameSummary;
    /*strings to indicate the current file name, whole file name, ending string of the file name, name of the output file*/

state_input:
    //inputting processes

    cout<<"Please insert the binary file name:"<<endl;
    cin>>FileNameChar; //file name without series number

    cout<<"Please insert the binary file name end:"<<endl;
    cin>>FileNameCharEnd; //file name without series number

    cout<<"Please insert the beginning file number:"<<endl;
    cin>>FileNameBeg; //starting series number

    cout<<"Please insert the end file number:"<<endl;
    cin>>FileNameEnd; //ending series number

    numOper = FileNameBeg - 1;
    //initializing the loop number

    OutputFileNameSummary =  FileNameChar;
    OutputFileNameSummary.append("OutputSummary.csv");
    // Define output file name

    ofstream OutputFileSummary;
    //file operation for the output

    OutputFileSummary.open(OutputFileNameSummary, ios::out | ios::trunc);

    if (!OutputFileSummary.is_open())
    {
        cout << "Could not open the output summary file!"<<endl;
        goto state_input;
    }

    do{
        numOper ++;

        currFileName = getNextFileName(FileNameChar, FileNameCharEnd, numOper);
        //Beginning series number
        NumofCounts = readOutFiveChannel(currFileName);
        //Get next file name
        OutputFileSummary <<* NumofCounts<<','<<* (NumofCounts+1)<<','<<* (NumofCounts+2)<<','<<*(NumofCounts+3)<<','<<* (NumofCounts+4)<<endl;
     }while(numOper<FileNameEnd); //read the files in series

    cout<<endl<<"File processing finished, please insert to operate:"<<endl<<endl<<"0. Quit"<<endl<<"1 Continue with next file"<<endl;
    cin>>numOper;
    if(numOper) {goto state_input;}

```

```
    OutputFileSummary.close();

    return 0;

}

/***************************************************************
function to get the next file name
***************************************************************/

string getNextFileName(string FileNameCharacters, string
FileNameCharactersEnd, int FileNameNum) {
    string getFileNameCharactersEnd, NextFileName;
    stringstream FileNameNumChar;
    getFileNameCharactersEnd = FileNameCharactersEnd;
    NextFileName = FileNameCharacters;
    FileNameNumChar << FileNameNum;
    NextFileName.append(FileNameNumChar.str());
    //Paste the series number on the file name
    NextFileName.append(getFileNameCharactersEnd);
    return NextFileName;
}

/***************************************************************
function for reading out the time-taggers
***************************************************************/

unsigned long * readOutFiveChannel(string sourceFileName) {

    string InputFileName, OutputFileNameCH1, OutputFileNameCH2, OutputFileNameCH3,
        OutputFileNameCH4,

OutputFileNameCH5, OutputFileNameCH6, OutputFileNameCH7;
    //define the input and output file names

    InputFileName = sourceFileName;
    InputFileName.append(".bin"); //input .bin file, without inserting ".bin"

    OutputFileNameCH1 = sourceFileName;
    OutputFileNameCH2 = sourceFileName;
    OutputFileNameCH3 = sourceFileName;
    OutputFileNameCH4 = sourceFileName;
    OutputFileNameCH5 = sourceFileName;
    OutputFileNameCH6 = sourceFileName;
    OutputFileNameCH7 = sourceFileName;

    OutputFileNameCH1.append("CH1.txt"); // Define output file name
    OutputFileNameCH2.append("CH2.txt");
    OutputFileNameCH3.append("CH3.txt");
    OutputFileNameCH4.append("CH4.txt");
    OutputFileNameCH5.append("CH5.txt");
    OutputFileNameCH6.append("CH6.txt");
    OutputFileNameCH7.append("CH7.txt");
    //output .txt file

    double buffer = 0;
    double channel = 0;
```

```
    double time = 0; //buffer variables

    unsigned long countsCH[7]={0};
    //array to count the total number of counts in each channel

    unsigned long * NumCounts = countsCH;

    ifstream InputFile;
    ofstream OutputFileCH1;
    ofstream OutputFileCH2;
    ofstream OutputFileCH3;
    ofstream OutputFileCH4;
    ofstream OutputFileCH5;
    ofstream OutputFileCH6;
    ofstream OutputFileCH7;

    InputFile.open(InputFileName, ios::in | ios::binary); //open the input file

    if (!InputFile.is_open())
    {
        cout << "Could not open source file!"<<endl;
        exit(1);
    }

    OutputFileCH1.open(OutputFileNameCH1, ios::out | ios::trunc);
    OutputFileCH2.open(OutputFileNameCH2, ios::out | ios::trunc);
    OutputFileCH3.open(OutputFileNameCH3, ios::out | ios::trunc);
    OutputFileCH4.open(OutputFileNameCH4, ios::out | ios::trunc);
    OutputFileCH5.open(OutputFileNameCH5, ios::out | ios::trunc);
    OutputFileCH6.open(OutputFileNameCH6, ios::out | ios::trunc);
    OutputFileCH7.open(OutputFileNameCH7, ios::out | ios::trunc);

    while (!InputFile.eof())
    {
        buffer = NULL;
        InputFile.read((char*)&buffer, sizeof(double));
        channel = (double)buffer;

        buffer = NULL;
        InputFile.read((char*)&buffer, sizeof(double));
        time = NULL;
        time = (double)buffer;

        countsCH[channel]++;
    }
    //read out and count the number of the time-taggers

    InputFile.close();
    OutputFileCH1.close();
    OutputFileCH2.close();
    OutputFileCH3.close();
    OutputFileCH4.close();
    OutputFileCH5.close();
    OutputFileCH6.close();
    OutputFileCH7.close();

    cout<<"File "<<InputFileName<<" processed."<<endl<<"Total number of counts:"<<endl
```

```
        <<"CH1:"<<countsCH[0]<<endl<<"CH2: "<<countsCH[1]<<endl<<"CH3:"<<countsCH[2]<<
        endl<<"CH4: "<<countsCH[3]<<endl<<"CH5: "<<countsCH[4]<<endl<<"CH6:"<<countsCH
        [5]<<endl<<"CH7: "<<countsCH[6]<<endl;

    return NumCounts;
}
```

A.2 source code: eraseTaggerBlocks.cpp

```
/***************************************************************
Program to erase blocks of the time-taggers in CH1 and CH2
with respect to a threshold value
by Daqing Wang, June 2012
***************************************************************/

#include <iostream>
#include <fstream>
#include <string>
#include <sstream>

using namespace std;

#define CH1 1
#define CH2 2
#define CH3 3
#define CH4 4
#define CH5 5
#define CH6 6
#define CH7 7
#define BIN_RESOULTION (1 / 6400000000)

unsigned long * eraseBackGround(string FileNameChar, string
sourceFileName, int thrsld);
//Function to to erase blocks of the time-taggers, input file name, return 0
string getNextFileName(string FileNameCharacters, string
FileNameCharactersEnd, int FileNameNum);
//Function to get next file name to process

/***************************************************************
main function
***************************************************************/

int main () {
    int numOper, FileNameBeg, FileNameEnd;
    int thrsldv;
    unsigned long * NumofCounts = NULL;

    string currFileName, FileNameChar, FileNameCharEnd, OutputFileNameErsBkgrd;

state_input:

    cout<<"Please insert the binary file name:"<<endl;
    cin>>FileNameChar; //File name without series number
    cout<<"Please insert the binary file name end:"<<endl;
    cin>>FileNameCharEnd; //File name without series number
    cout<<"Please insert the beginning file number:"<<endl;
```

```
    cin>>FileNameBeg; //Starting series number
    cout<<"Please insert the end file number:"<<endl;
    cin>>FileNameEnd; //Ending series number
    cout<<"Please insert the thresold value for erasing the background:"<<endl;
    cin>>thrsldv; //Thresold value

    numOper = FileNameBeg - 1;

    do{
        numOper ++;
        currFileName = getNextFileName(FileNameChar, FileNameCharEnd, numOper);
        //Beginning series number
        NumofCounts = eraseBackGround(FileNameChar, currFileName, thrsldv);
        //Get next file name
    }while(numOper<FileNameEnd);

    cout<<endl<<"File processing finished, please insert to operate:"<<endl<<endl<<"0. Quit"<<endl<<"1. Continue with next file"<<endl;
    cin>>numOper;
    if(numOper) {goto state_input;}

    return 0;
}

/*************************************************************
function to get the next file name
*************************************************************/

string getNextFileName(string FileNameCharacters, string
FileNameCharactersEnd, int FileNameNum) {
    string getFileNameCharactersEnd, NextFileName;
    stringstream FileNameNumChar;
    getFileNameCharactersEnd = FileNameCharactersEnd;
    NextFileName = FileNameCharacters;
    FileNameNumChar << FileNameNum;
    NextFileName.append(FileNameNumChar.str());
    //Paste the series number on the file name
    NextFileName.append(getFileNameCharactersEnd);
    return NextFileName;
}

/*************************************************************
Erase the time-taggers according to the counts in independent
channels
*************************************************************/

unsigned long * eraseBackGround(string tempFileNameChar, string
sourceFileName, int thrsld) {

    string InputFileName, OutputFileName, OutputSummaryFileName;
    stringstream FileNameThrsVal;
    int tagger[15] = {0, 240, 63, 0, 64, 0, 0, 0, 0, 0, 0, 24, 64, 28, 64};
    //indentifer of the two channels
    int numOfCountsCH1, numOfCountsCH2, numOfCountsTotal;
    int thrsldVlue = thrsld;
    int loopnum = 0;
    double buffer0 = 0;
```

```
    double buffer[BUFFERSIZE] = {0};

    int buffer_chan[BUFFERSIZE] = {0};
    double bufferStart, bufferEnd;
    InputFileName = sourceFileName;
    InputFileName.append(".bin");

    OutputFileName = sourceFileName;
    OutputFileName.append("thrsld_");

    FileNameThrsVal << thrsldVlue;
    OutputFileName.append(FileNameThrsVal.str());
    OutputFileName.append(".bin");

    OutputSummaryFileName = tempFileNameChar;
    OutputSummaryFileName.append(FileNameThrsVal.str());
    OutputSummaryFileName.append("Summary.csv");

    double channel = 0;
    double time = 0;
    numOfCountsCH1 = 0;
    numOfCountsCH2 = 0;
    numOfCountsTotal = 0;

    bufferStart = 0;
    bufferEnd = 0;

    unsigned long countsCH[8]={0};
    unsigned long countsErasedCH[8]={0};

    ifstream InputFile;
    ofstream OutputFile;
    ofstream OutputSummaryFile;

    InputFile.open(InputFileName, ios::in | ios::binary);

    if (!InputFile.is_open())
    {
        cout << "Could not open source file!"<<endl;
        exit(1);
    }

    OutputFile.open(OutputFileName, ios::out | ios::trunc | ios::binary);

    while (!InputFile.eof())
    {
        buffer0 = NULL;
        InputFile.read((char*)&buffer0, sizeof(double));
        channel = (double)buffer0;

        buffer0 = NULL;
        InputFile.read((char*)&buffer0, sizeof(double));
        time = NULL;
        time = (double)buffer0;
        buffer[numOfCountsTotal] = time;
        buffer_chan[numOfCountsTotal]=channel;
        countsCH[channel]++;
```

```
        numOfCountsTotal++;
        bufferEnd = time;

        if(bufferEnd - bufferStart >= 320000000)
        {
            if(numOfCountsTotal>=BUFFERSIZE) {cout<<"Two much counts in one interval,
                please change the parameters!"<<endl;}
            if((numOfCountsCH1 >= thrsld)&&(numOfCountsCH2 >= thrsld))
            {
                for(loopnum=0; loopnum<numOfCountsTotal; loopnum++)
                {
                    if(buffer_chan[loopnum]==CH0)
                    {
                        OutputFile.write((char*)(&tagger[0]),1);
                        OutputFile.write((char*)(&tagger[0]),1);
                        OutputFile.write((char*)(&tagger[0]),1);
                        OutputFile.write((char*)(&tagger[0]),1);
                        OutputFile.write((char*)(&tagger[0]),1);
                        OutputFile.write((char*)(&tagger[0]),1);
                        OutputFile.write((char*)(&tagger[0]),1);
                        OutputFile.write((char*)(&tagger[0]),1);
                        OutputFile.write((char*)(&buffer[loopnum]),8);
                        countsErasedCH[0]++;
                    }
                    if(buffer_chan[loopnum]==CH1)
                    {
                        OutputFile.write((char*)(&tagger[0]),1);
                        OutputFile.write((char*)(&tagger[0]),1);
                        OutputFile.write((char*)(&tagger[0]),1);
                        OutputFile.write((char*)(&tagger[0]),1);
                        OutputFile.write((char*)(&tagger[0]),1);
                        OutputFile.write((char*)(&tagger[0]),1);
                        OutputFile.write((char*)(&tagger[1]),1);
                        OutputFile.write((char*)(&tagger[2]),1);
                        OutputFile.write((char*)(&buffer[loopnum]),8);
                        countsErasedCH[1]++;
                    }
                    if(buffer_chan[loopnum]==CH2)
                    {
                        OutputFile.write((char*)(&tagger[0]),1);
                        OutputFile.write((char*)(&tagger[0]),1);
                        OutputFile.write((char*)(&tagger[0]),1);
                        OutputFile.write((char*)(&tagger[0]),1);
                        OutputFile.write((char*)(&tagger[0]),1);
                        OutputFile.write((char*)(&tagger[0]),1);
                        OutputFile.write((char*)(&tagger[3]),1);
                        OutputFile.write((char*)(&tagger[4]),1);
                        OutputFile.write((char*)(&buffer[loopnum]),8);
                        countsErasedCH[2]++;
                    }
                    if(buffer_chan[loopnum]==CH6)
                    {
                        OutputFile.write((char*)(&tagger[0]),1);
                        OutputFile.write((char*)(&tagger[0]),1);
                        OutputFile.write((char*)(&tagger[0]),1);
                        OutputFile.write((char*)(&tagger[0]),1);
```

```
                        OutputFile.write((char*)(&tagger[0]),1);
                        OutputFile.write((char*)(&tagger[0]),1);
                        OutputFile.write((char*)(&tagger[11]),1);
                        OutputFile.write((char*)(&tagger[12]),1);
                        OutputFile.write((char*)(&buffer[loopnum]),8);
                        countsErasedCH[6]++;
                    }
                    if(buffer_chan[loopnum]==CH7)
                    {
                        OutputFile.write((char*)(&tagger[0]),1);
                        OutputFile.write((char*)(&tagger[0]),1);
                        OutputFile.write((char*)(&tagger[0]),1);
                        OutputFile.write((char*)(&tagger[0]),1);
                        OutputFile.write((char*)(&tagger[0]),1);
                        OutputFile.write((char*)(&tagger[0]),1);
                        OutputFile.write((char*)(&tagger[13]),1);
                        OutputFile.write((char*)(&tagger[14]),1);
                        OutputFile.write((char*)(&buffer[loopnum]),8);
                        countsErasedCH[7]++;
                    }
                }
            }
            if((numOfCountsCH1 >= thrsld)&&(numOfCountsCH2 < thrsld))
            {/*Repeating codes for writing the taggers omitted here due to space
                limitation*/}
            if((numOfCountsCH1 < thrsld)&&(numOfCountsCH2 >= thrsld))
            {/*Repeating codes for writing the taggers omitted here due to space
                limitation*/}
            if((numOfCountsCH1 < thrsld)&&(numOfCountsCH2 < thrsld))
            {/*Repeating codes for writing the taggers omitted here due to space
                limitation*/}

            bufferStart = bufferEnd;
            numOfCountsTotal = 0;
            numOfCountsCH1 = 0;
            numOfCountsCH2 = 0;
            memset(buffer,0,500*sizeof(unsigned long));
            memset(buffer_chan,0,500*sizeof(unsigned long));
        }
    }

/**************************************************************
Final processing and output
**************************************************************/

    InputFile.close();
    OutputFile.close();

    cout<<"File "<<InputFileName<<" processed."<<endl<<"Orginal number of counts:"<<
        endl<<"CH0: "<<countsCH[0]<<'\t'<<"CH1: "<<countsCH[1]<<'\t'<<"CH2: "<<
        countsCH[2]<<'\t'<<"CH3: "<<countsCH[3]<<'\t'<<"CH4: "<<countsCH[4]<<'\t'<<"
        CH5: "<<countsCH[5]<<'\t'<<"CH6: "<<countsCH[6]<<'\t'<<"CH7: "<<countsCH[7]<<
        endl;
    cout<<"Number of Counts after erasing:"<<endl<<"CH0: "<<countsErasedCH[0]<<'\t'<<"
        CH1: "<<countsErasedCH[1]<<'\t'<<"CH2: "<<countsErasedCH[2]<<'\t'<<"CH3: "<<
        countsErasedCH[3]<<'\t'<<"CH4: "<<countsErasedCH[4]<<'\t'<<"CH5: "<<
        countsErasedCH[5]<<'\t'<<"CH6: "<<countsErasedCH[6]<<'\t'<<"CH7: "<<countsCH
```

```
        [7]<<endl;

    OutputSummaryFile.open(OutputSummaryFileName, ios::app);
    OutputSummaryFile <<countsCH[0]<<','<<countsCH[1]<<','<<countsCH[2]<<','<<countsCH[3]<<','<<countsCH[4]<<','<<countsCH[5]<<','<<countsCH[6]<<','<<countsCH[7]<<','<<countsErasedCH[0]<<','<<countsErasedCH[1]<<','<<countsErasedCH[2]<<','<<countsErasedCH[3]<<','<<countsErasedCH[4]<<','<<countsErasedCH[5]<<','<<countsErasedCH[6]<<','<<countsErasedCH[7]<<','<<endl;
    OutputSummaryFile.close();

    unsigned long * NumCounts = countsCH;

    return NumCounts;
}
```

A.3 source code: processingCSVFiles.cpp

```
/*************************************************************
Program for collectively processing the outputed CSV files
by Daqing Wang, July 2012
*************************************************************/
#include <iostream>
#include <fstream>
#include <string>
#include <sstream>
#include <cstdlib>

using namespace std;

#define CH1 1
#define CH2 2
#define CH3 3
#define CH4 4
#define CH5 5
#define CH6 6
#define CH7 7
#define M_LENGTH 2000
#define M_WIDTH 27

extern double result[5] = {0};

double * readCSVfiles(string sourceFileName);
//Function to read out csv files into an array
string getNextFileName(string FileNameCharacters, string
FileNameCharactersEnd, int FileNameNum);
//Function to get next file name to process

/*************************************************************
main function
*************************************************************/
int main () {
    int numOper, FileNameBeg, FileNameEnd;
    double * NumofCounts = NULL;

    string currFileName, FileNameChar, FileNameCharEnd, OutputFileNameSummary;

```

```cpp
state_input:

    cout<<"Please insert the binary file name:"<<endl;
    cin>>FileNameChar; //File name without series number
    cout<<"Please insert the binary file name end:"<<endl;
    cin>>FileNameCharEnd; //File name without series number
    cout<<"Please insert the beginning file number:"<<endl;
    cin>>FileNameBeg; //Starting series number
    cout<<"Please insert the end file number:"<<endl;
    cin>>FileNameEnd; //Ending series number

    numOper = FileNameBeg - 1;

    OutputFileNameSummary =  FileNameChar;
    OutputFileNameSummary.append("OutputSummary.csv"); // Define output file name

    ofstream OutputFileSummary;

    OutputFileSummary.open(OutputFileNameSummary, ios::out | ios::trunc);

    if (!OutputFileSummary.is_open())
    {
        cout << "Could not open the output summary file!"<<endl;
        goto state_input;
    }

    do{
        numOper ++;

        currFileName = getNextFileName(FileNameChar, FileNameCharEnd, numOper); // Beginning series number
        NumofCounts = readCSVfiles(currFileName); //Get next file name
        OutputFileSummary <<* NumofCounts<<','<<* (NumofCounts+1)<<','<<* (NumofCounts+2)<<','<<* (NumofCounts+3)<<','<<* (NumofCounts+4)<<','<<* (NumofCounts+5)<<endl;
    }while(numOper<FileNameEnd);

    cout<<endl<<"File processing finished, please insert to operate:"<<endl<<endl<<"0. Quit"<<endl<<"1 Continue with next file"<<endl;
    cin>>numOper;
    if(numOper) {goto state_input;}
    OutputFileSummary.close();

    return 0;

}

/***************************************************************
function to get the next file name
***************************************************************/

string getNextFileName(string FileNameCharacters, string
FileNameCharactersEnd, int FileNameNum) {
    string getFileNameCharactersEnd, NextFileName;
    stringstream FileNameNumChar;
    getFileNameCharactersEnd = FileNameCharactersEnd;
    NextFileName = FileNameCharacters;
```

```
    FileNameNumChar << FileNameNum;
    NextFileName.append(FileNameNumChar.str());
    //Paste the series number on the file name
    NextFileName.append(getFileNameCharactersEnd);
    return NextFileName;
}

/**************************************************************
function to read and process the CSV files
**************************************************************/
double * readCSVfiles(string sourceFileName) {
    string InputFileName;
    InputFileName = sourceFileName;

    string str_buf;
    int buffer[M_LENGTH][M_WIDTH] = {0};
    int buffer0 = 0;
    int i=0, j=0;
    double noise0 = 0, noise1 = 0;
    double SNR0 = 0, SNR1 = 0;

    ifstream InputFile;

    InputFile.open(InputFileName, ios::in);

    if (!InputFile.is_open())
    {
        cout << "Could not open source file!"<<endl;
        exit(1);
    }

    while (!InputFile.eof())
    {
        for(i=0; i<M_LENGTH-1; i++)
        {
            getline(InputFile, str_buf);
            istringstream stream(str_buf);
            for(j=0; j<M_WIDTH-1; j++)
            {
                getline(stream, str_buf, ',');
                buffer[i][j] = atoi(str_buf.c_str());
            }
        }
        break;
    }

    InputFile.close();
    InputFile.clear();

    /**********************************************************
    File processing, sorting files from largest to smallest
    **********************************************************/

    for(i=M_LENGTH-1; i>0; i--)
        for(j=i; j>0; j--)
        {
            if(buffer[j][3]>buffer[j-1][3])
```

```
            {
                buffer0 = buffer[j][3];
                buffer[j][3] = buffer[j-1][3];
                buffer[j-1][3] = buffer0;
                buffer0 = 0;
            }
        }

        for(i=M_LENGTH-1; i>0; i--)
            for(j=i; j>0; j--)
            {
                if(buffer[j][8]>buffer[j-1][8])
                {
                    buffer0 = buffer[j][8];
                    buffer[j][8] = buffer[j-1][8];
                    buffer[j-1][8] = buffer0;
                    buffer0 = 0;
                }
            }

            for(i=1;i<11;i++)
            {
                noise0 += buffer[i][3];
                noise1 += buffer[i][8];
            }

            noise0 /= 10;
            noise1 /= 10;

            SNR0 = buffer[0][3]/noise0;
            SNR1 = buffer[0][8]/noise1;

            result[0] = buffer[0][3];
            result[1] = buffer[0][8];
            result[2] = noise0;
            result[3] = noise1;
            result[4] = SNR0;
            result[5] = SNR1;

            cout<<" Signal = "<<buffer[0][3]<<", "<<buffer[0][8]<<"\t"<<"Noise = "<<
                noise0<<", "<<noise1<<"\t"<<"SNR = "<<SNR0<<", "<<SNR1<<endl;

            return result;
}
```

Appendix B

Steps on building up a receiver's module in the OGS

1. Setup the local alignment laser behind the blue wall of the pizza oven
   - Adjust the divergence of the OGS ($f = 40$ m), to focal at the right position
   - Set up pinholes along the bench to mark the beam direction
   - Set up dichroic mirror (HT532, HR 808 and 1064) on the indexers
   - Set up the re-collimation lens ($f = 40$ cm), before the dichroic mirrors and exactly 40 cm away from the field stop
   - Setup the $3x$ telescope with lenses of 150 mm and 50 mm and make sure the beam still going right through the pinholes
   - This is only pre-adjustment to know about where the beam should be. Final adjustment should be finished with the La Palma link
2. Adjust with the light from La Palma
   - The pinholes and mirrors should be adjusted until the final fixing of the divergence and direction
   - OGS adjusted to the right focus (13.8 mm)
   - Set the OGS tracking point (approximately in the middle of the field stop)
   - Set in dichroic mirror and $f = 40$cm lens across the widest possible distance (via a mirror)
   - Set the 3x telescope and the 4 mm beam over the widest possible distance
3. Adjust with local laser (insert local laser on the remote laser)

- Now pinholes / lenses / mirror in the La Palma links must not be re-adjusted, and the local adjustment setup should be adjusted correspondingly
- Adjust the APDs (active area = 0.5 mm) at the center of the focal spots (D = 0.03 mm)

4. Setting the focus with the La Palma link (minimize spot size)
   - With the strong alignment 808 nm light from La Palma, adjust the focus by looking at the dancing spot with an IF viewer
   - Adjust the X, Y position by looking at the count rates

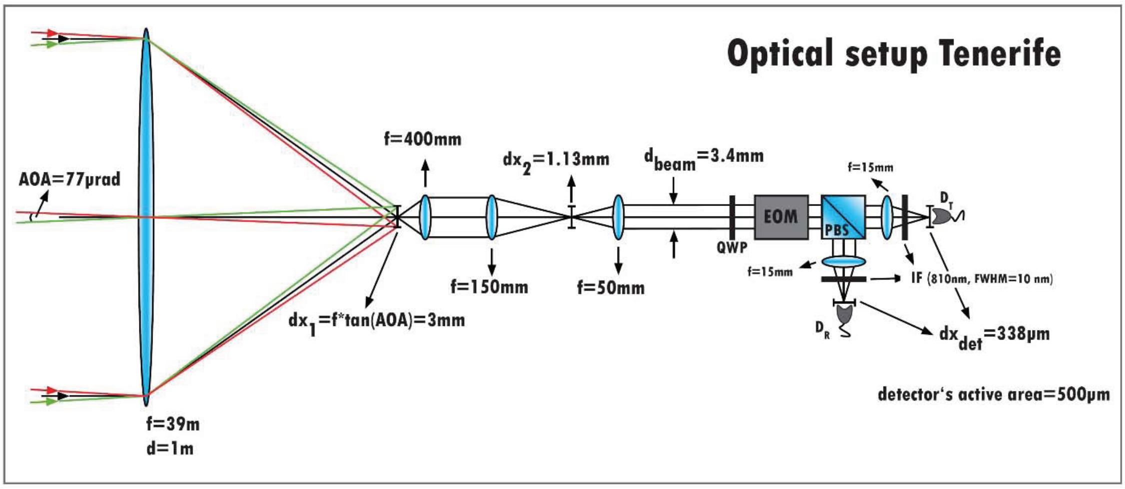

Figure B.1: Optical design of the Optical Ground Station (OGS) and the receiver's module in Tenerife. Taken from [40].

Appendix C

Steps on operating the OGS tracking system

1. Open the CCD camera in the Coude room under the black box
2. Set the switch box (on the wooden weather station) to CR1
3. Login the control computer
4. TCC set as remote (click TCP/IP clicken and then SELECT)
5. PC select configuration: "Zoran_Caude", check whether it has connection to TEL und CAM (in green)
6. GUIDING-WINDOW:
   - Click "Coude on-axis guiding"
   - Search box should be 300, then press INIT
7. CAMERA BASE-WINDDOW:
   - Uncheck File index
   - Uncheck Incr.
   - Set camera to -30 ℃
   - Check PLOT
   - Exposure time set to 1-2 second (you may attenuate the laser from La Palma)
   - Press SET every time you change something in this window
8. GUIDING-WINDOW:
   - Put current and new position to 600. It's the center of the CCD

- Press plot to see the spot on the CCD
- 65000 is the saturation value, keep below that
- Press POSITION (TCC will follow the NEW POSITION value)

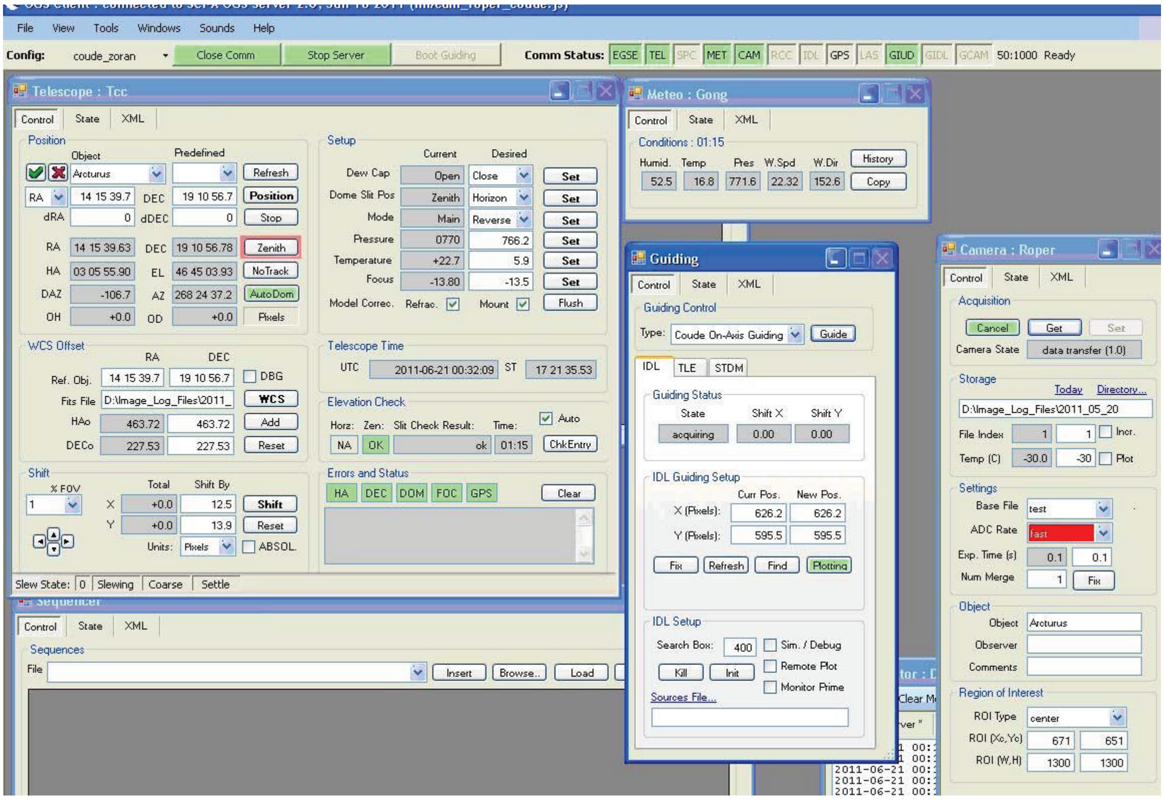

Figure C.1: Screenshot of the control software of the OGS tracking system.

Bibliography

[1] A. Einstein, B. Podolsky and N. Rosen. Can quantum-mechanical description of physical reality be considered complete? *Phys. Rev.* **47**, 777-780, 1935.

[2] J.S. Bell. On the Einstein Poldolsky Rosen paradox. *Physics* **1**, 195-200, 1964.

[3] S.J. Freedman and J.F. Clauser. Experimental test of local hidden-variable theories. *Phys. Rev. Lett.* **28**, 938-941, 1972.

[4] A. Aspect, P. Grangier and G. Roger. Experimental tests of realistic local theories via Bell's theorem. *Phys. Rev. Lett.* **47**, 460-463, 1981.

[5] A. Aspect, J. Dalibard and G. Roger. Experimental test of Bell's inequalities using time-varying analyzers. *Phys. Rev. Lett.* **49**, 1804-1807, 1982.

[6] A. Aspect, P. Grangier and G. Roger. Experimental realization of Einstein-Podolsky-Rosen-Bohm Gedankenexperiment: A new violation of Bell's inequalities. *Phys. Rev. Lett.* **49**, 91-94, 1982.

[7] C.H. Bennett, G. Brassard, C. Crépeau, R. Jozsa, A. Peres and W. K.Wootters. Teleporting an unknown quantum state via dual classical and Einstein-Podolsky-Rosen channels. *Phys. Rev. Lett.* **70**, 1895-1899, 1993.

[8] D. Bouwmeester, J.-W. Pan, K. Mattle, M. Eibl, H. Weinfurter and A. Zeilinger. Experimental quantum teleportation. *Nature* **390**, 575-579, 1997.

[9] J.-W. Pan, Z.-B. Chen, C.-Y. Lu, H. Weinfurter, A. Zeilinger and M.Žukowski. Multiphoton entanglement and interferometry, *Rev. Mod. Phys.* **84**, 777-838, 2012.

[10] S. Massar and S. Popescu. Optimal extraction of information from infinite quantum ensembles. *Phys. Rev. Lett.* **74**, 1259-1262, 1995.

[11] D. Boschi, S. Branca, F. De Martini, L. Hardy and S. Popescu. Experimental realization of releporting an unknown pure quantum state via dual classical and Einstein-Podolsky-Rosen channels. *Phys. Rev. Lett.* **80**, 1121-1125, 1998.

[12] A. Furusawa, J.L. Sørensen, S.L. Braunstein, C.A. Fuchs, H.J. Kimble and E.S. Polzik.

Unconditional quantum teleportation. *Science* **282**, 706-709, 1998.

[13] M.A. Nielsen, E. Knill and R. Laflamme. Complete quantum teleportation using nuclear magnetic resonance. *Nature* **396**, 52-55, 1998.

[14] M.D. Barrett, J. Chiaverini, T. Schaetz, J. Britton, W.M. Itano, J.D. Jost, E. Knill, C. Langer, D. Leibfried, R. Ozeri and D. J. Wineland. Deterministic quantum teleportation of atomic qubits. *Nature* **429**, 737-739, 2004.

[15] J.F. Sherson, H. Krauter, R.K. Olsson, B. Julsgaard, K. Hammerer, I. Cirac and E.S. Polzik. Quantum teleportation between light and matter. *Nature* **443**, 557-560, 2006.

[16] I. Marcikic, H. de Riedmatten, W. Tittel, H. Zbinden and N. Gisin. Long distance teleportation of qubits at telecommunication wavelengths. *Nature* **421**, 509-513, 2003.

[17] R. Ursin, T. Jennewein, M. Aspelmeyer, R. Kaltenbaek, M. Lindenthal, P. Walther and A. Zeilinger. Communications: Quantum teleportation across the Danube. *Nature* **430**, 849, 2004.

[18] R.J. Hughes, W.T. Buttler, P.G. Kwiat, S.K. Lamoreaux, G.L. Morgan, J.E. Nordholt and C.G. Peterson. Free-space quantum key distribution in day light. *J. Mod. Opt.* **47**, 549-562, 2000.

[19] J.G. Rarity, P.R. Tapster, P.M. Gorman and P. Knight. Ground to satellite secure key exchange using quantum cryptography. *N. J. Phys.* **4**, 82, 2002.

[20] M. Aspelmeyer, H.R. Böhm, T. Gyatso, T. Jennewein, R. Kaltenbaek, M. Lindenthal, G. Molina-Terriza, A. Poppe, K. Resch, M. Taraba, R. Ursin, P. Walther and A. Zeilinger. Long-distance free-space distribution of quantum entanglement. *Science* **301**, 621-623, 2003.

[21] I. Marcikic, A. Lamas-Linares and C. Kurtsiefer. Free-space quantum key distribution with entangled photons. *Appl. Phys. Lett.* **89**, 101122, 2006.

[22] P. Villoresi, T. Jennewein, F. Tamburini, M. Aspelmeyer, C. Bonato, R. Ursin, C. Pernechele, V. Luceri, G. Bianco, A. Zeilinger and C. Barbieri. Experimental verification of the feasibility of a quantum channel between space and Earth. *N. J. Phys.* **10**, 033038, 2008.

[23] T. Scheidl, R. Ursin, A. Fedrizzi, S. Ramelow, X.-S. Ma, T. Herbst, R. Prevedel, L. Ratschbacher, J. Kofler, T. Jennewein and A. Zeilinger. Feasibility of 300 km quantum key distribution with entangled states. *N. J. Phys.* **11**, 085002, 2009.

[24] X.-M. Jin, J.-G. Ren, B. Yang, Z.-H. Yi, F. Zhou, X.-F. Xu, S.-K. Wang, D. Yang, Y.-F. Hu, S. Jiang, T. Yang, H. Yin, K. Chen, C.-Z. Peng and J.-W. Pan. Experimental free-space quantum teleportation. *Nature Photon.* **4**, 376-381, 2010.

[25] R. Ursin, F. Tiefenbacher, T. Schmitt-Manderbach, H. Weier, T. Scheidl, M. Lindenthal, B. Blauensteiner, T. Jennewein, J. Perdigues, P. Trojek, B. Ömer, M. Fürst, M. Meyenburg, J. Rarity, Z. Sodnik, C. Barbieri, H. Weinfurter and A. Zeilinger. Entanglement-based quantum communication over 144 km. *Nature Phys.* **3**, 481-486, 2007.

[26] A. Fedrizzi, R. Ursin, T. Herbst, M. Nespoli, R. Prevedel, T. Scheidl, F. Tiefenbacher, T. Jennewein and A. Zeilinger. High-fidelity transmission of entanglement over a high-loss free-space channel. *Nature Phys.* **5**, 389-392, 2009.

[27] T. Scheidl, R. Ursin, J. Kofler, S. Ramelow, X.-S. Ma, T. Herbst, L. Ratschbacher, A. Fedrizzi, N.K. Langford, T. Jennewein and A. Zeilinger. Violation of local realism with freedom of choice. *Proc. Natl. Acad. Sci. USA* **107**, 19708-19713, 2010.

[28] X.-S. Ma, T. Herbst, T. Scheidl, D. Wang, S. Kropatschek, W. Naylor, B. Wittmann, A. Mech, J. Kofler, E. Anisimova, V. Makarov, T. Jennewein, R. Ursin and A. Zeilinger. Quantum teleportation over 143 kilometres using active feed-forward. *Nature* **489**, 269-273, 2012.

[29] J. Clauser and A. Shimony. Bell's theorem: experimental tests and implications. *Rep. Prog. Phys.* **41**, 1881-1927, 1978.

[30] P.G. Kwiat, K. Mattle, H. Weinfurter, A. Zeilinger, A.V. Sergienko and Y.H. Shih. New high-intensity source of polarization-entangled photon pairs. *Phys. Rev. Lett.* **75**, 4337-4341, 1995.

[31] J.B. Altepeter, E. Jeffrey and P.G. Kwiat. Phase-compensated ultra-bright source of entangled photons, *Opt. Exp.* **13**, 8951-8959, 2005.

[32] T.E. Keller and M.H. Rubin. Theory of two-photon entanglement for spontaneous parametric down-conversion driven by a narrow pump pulse. *Phys. Rev. A* **56**, 1534-1541, 1997.

[33] W.P. Grice and I.A. Walmsley. Spectral information and distinguishability in type-II down-conversion with a broadband pump. *Phys. Rev. A* **56**, 1627-1634, 1997.

[34] H.-S. Poh, J. Lim, I. Marcikic, A. Lamas-Linares and C. Kurtsiefer. Eliminating spectral distinguishability in ultrafast spontaneous parametric down-conversion. *Phys. Rev. A* **80**, 043815, 2009.

[35] X.-C. Yao, T.-X. Wang, P. Xu, H. Lu, G.-S. Pan, X.-H. Bao, C.-Z. Peng, C.-Y. Lu, Y.-A. Chen and J.-W. Pan. *Nature Photon.* **6**, 225-228, 2012.

[36] J. Calsamiglia and N. Lütkenhaus. Maximum efficiency of a linear-optical Bell-state analyzer. *Appl. Phys. B* **72**, 67-71, 2001.

[37] Y.-S. Kim, Y.-C. Jeong, S. Sauge, V. Makarov and Y.-H. Kim. Ultra-low noise single-photon detector based on Si avalanche photodiode. *Rev. Sci. Instrum.* **82**, 093110, 2011.

[38] A.G. White, D.F.V. James, P.H. Eberhard and P.G. Kwiat. Nonmaximally entangled states: production, characterization, and utilization. *Phys. Rev. Lett.* **83**, 3103-3107, 1999.

[39] Trimble Navigation Limited Mobile and Timing Technologies. ThunderBolt GPS Disciplined Clock Manual. *Data sheet*, 2000.

[40] T. Scheidl. A fundamental test and an application of quantum entanglement. *Dissertation*, Universität Wien, 2009.